JGR Atmospheres

RESEARCH ARTICLE
10.1029/2022JD037177

Special Section:
Fire in the Earth System

Wildfire Smoke Influence on Cloud Water Chemical Composition at Whiteface Mountain, New York

Jamy Y. Lee[1], Peter K. Peterson[1,2], Logan R. Vear[1], Ryan D. Cook[1], Amy P. Sullivan[3], Ellie Smith[4], Lelia N. Hawkins[4], Nicole E. Olson[1], Rachel Hems[1], Philip K. Snyder[5], and Kerri A. Pratt[1,6]

[1]Department of Chemistry, University of Michigan, Ann Arbor, MI, USA, [2]Now at Department of Chemistry, Whittier College, Whittier, CA, USA, [3]Department of Atmospheric Science, Colorado State University, Fort Collins, CO, USA, [4]Department of Chemistry, Harvey Mudd College, Claremont, CA, USA, [5]Adirondack Lake Survey Corporation, Ray Brook, NY, USA, [6]Department of Earth and Environmental Sciences, University of Michigan, Ann Arbor, MI, USA

Abstract Wildfires significantly impact air quality and climate, including through the production of aerosols that can nucleate cloud droplets and participate in aqueous-phase reactions. Cloud water was collected during the summer months (June–September) of 2010–2017 at Whiteface Mountain, New York and examined for biomass burning influence. Cloud water samples were classified by their smoke influence based on backward air mass trajectories and satellite-detected smoke. A total of 1,338 cloud water samples collected over 485 days were classified by their probability of smoke influence, with 49% of these days categorized as having moderate to high probability of smoke influence. Carbon monoxide and ozone levels were enhanced during smoke influenced days at the summit of Whiteface Mountain. Smoke-influenced cloud water samples were characterized by enhanced concentrations of potassium, sulfate, ammonium, and total organic carbon, compared to samples lacking identified influence. Five cloud water samples were examined further for the presence of dissolved organic compounds, insoluble particles, and light-absorbing components. The five selected cloud water samples contained the biomass burning tracer levoglucosan at 0.02–0.09 μM. Samples influenced by air masses that remained aloft, above the boundary layer during transport, had lower insoluble particle concentrations, larger insoluble particle diameters, and larger oxalate:sulfate ratios, suggesting cloud processing had occurred. These findings highlight the influence that local and long-range transported smoke have on cloud water composition.

Plain Language Summary Wildfires significantly impact air quality and climate, including through the production of smoke particles that can form clouds. Cloud water at Whiteface Mountain, New York during summer is frequently influenced by transported smoke from wildfires. This study examined 8 years of cloud water chemical composition data with support from air mass modeling and satellite-detected smoke. These results are important in the context of increasing wildfires in recent years.

Key Points:

- Local and transported smoke influenced 49% of summertime cloud water samples
- Potassium, sulfate, ammonium, and total organic carbon were enhanced in smoke-influenced cloud water
- Ozone and carbon monoxide levels were elevated at the summit of Whiteface Mountain during periods with high probability of smoke influence

Supporting Information:

Supporting Information may be found in the online version of this article.

Correspondence to:

K. A. Pratt,
prattka@umich.edu

Citation:

Lee, J. Y., Peterson, P. K., Vear, L. R., Cook, R. D., Sullivan, A. P., Smith, E., et al. (2022). Wildfire smoke influence on cloud water chemical composition at Whiteface Mountain, New York. *Journal of Geophysical Research: Atmospheres*, *127*, e2022JD037177. https://doi.org/10.1029/2022JD037177

Received 23 MAY 2022
Accepted 26 SEP 2022

Author Contributions:

Conceptualization: Kerri A. Pratt
Formal analysis: Jamy Y. Lee, Logan R. Vear, Ryan D. Cook
Funding acquisition: Kerri A. Pratt
Investigation: Jamy Y. Lee, Peter K. Peterson, Logan R. Vear, Ryan D. Cook, Amy P. Sullivan, Ellie Smith, Lelia N. Hawkins, Nicole E. Olson
Methodology: Peter K. Peterson

1. Introduction

Fire activity in North America has drastically increased in recent years (Dennison et al., 2014; Flannigan et al., 2013; Jolly et al., 2015; Liu et al., 2016; Tymstra et al., 2020; Westerling, 2016). Wild, prescribed, and agricultural fires are a large source of particulate matter less than 2.5 μm in diameter ($PM_{2.5}$) (Jaffe et al., 2020; Larsen et al., 2018; O'Dell et al., 2021), including to the free troposphere (Hung et al., 2021). $PM_{2.5}$ degrades air quality (Brey, Barnes, et al., 2018; Liu et al., 2016) and has been linked to chronic health problems (Matz et al., 2020; O'Dell et al., 2021). Additionally, $PM_{2.5}$ impacts climate through the direct aerosol effect, where aerosols scatter or absorb solar radiation (Ghan et al., 2012; Haywood & Boucher, 2000), and through the aerosol indirect effect by modifying the radiative properties of clouds (Haywood & Boucher, 2000; Lohmann & Feichter, 2005). Simulations using the Weather Research and Forecast modeling system with Chemistry (WRF-Chem-SMOKE) for northern Canada (Lu & Sokolik, 2013) and the western United States (Twohy et al., 2021) show that clouds significantly influenced by biomass burning smoke have increased cloud droplet number concentrations and decreased cloud droplet sizes. In this way, biomass burning particles can delay the onset of precipitation, affecting the lifetime, chemistry, and microphysical properties of clouds (Andreae et al., 2004; Ge et al., 2014; Grandey et al., 2016; Lee & Wang, 2020; Lu & Sokolik, 2013).

Project Administration: Kerri A. Pratt
Resources: Philip K. Snyder, Kerri A. Pratt
Supervision: Peter K. Peterson, Lelia N. Hawkins, Kerri A. Pratt
Writing – original draft: Jamy Y. Lee
Writing – review & editing: Peter K. Peterson, Amy P. Sullivan, Lelia N. Hawkins, Rachel Hems, Philip K. Snyder, Kerri A. Pratt

The chemical composition of biomass burning particles influences their interactions with radiation and ability to uptake water, affecting their potential for aqueous phase reactions (Ahern et al., 2019; Cook et al., 2017; Ervens et al., 2004, 2011; Gilardoni et al., 2016; Schurman et al., 2018). The chemical composition of smoke can vary based on vegetation type, burn conditions, and meteorological conditions (Chen et al., 2017; Gilman et al., 2015). Fresh biomass burning particles typically consist of greater than ~80%, by mass, organic carbon, with minor mass contributions from black carbon and potassium salts, including sulfate, chloride, and nitrate (Kleinman et al., 2020; Liu et al., 2017; May et al., 2014; Reid et al., 2005; Thepnuan et al., 2019; Zhou et al., 2017). Previous single-particle mass spectrometry studies characterize freshly emitted smoke particles as having prominent ions corresponding to potassium, sulfate, and nitrate (Hudson et al., 2004; Pratt et al., 2011; Silva et al., 1999; Zauscher et al., 2013). These fresh smoke particles have been identified as cloud condensation nuclei (CCN) (Bougiatioti et al., 2016; Engelhart et al., 2012; Petters, Carrico, et al., 2009), and ice nucleating particles (INPs) (McCluskey et al., 2014; Petters, Parsons, et al., 2009), thereby impacting cloud formation and properties (Penner et al., 1992; Reid et al., 2005; Spracklen et al., 2011).

During atmospheric transport, biomass burning emissions are typically oxidized by hydroxyl radicals, producing secondary organic aerosol (Ahern et al., 2019; Lim et al., 2019). Secondary species, such as ammonium, nitrate, sulfate, and oxidized organics are often incorporated onto existing smoke particles (Chen et al., 2017; Engelhart et al., 2012; Pratt et al., 2010; Vakkari et al., 2014). The chemical processing of biomass burning particles increases CCN activity (Desyaterik et al., 2013; Hodshire et al., 2019; Reid et al., 2005; Zhou et al., 2017) by increasing the hydrophilicity of the particles through chemical oxidation and addition of soluble components (e.g., sulfate, nitrate, and oxidized organics) (Jing et al., 2018; Khalizov et al., 2009; Leskinen et al., 2007; Pósfai et al., 2003). Once incorporated into clouds, these chemical changes are reflected on the single-particle level. Smoke influenced cloud droplet residual particles characterized by scanning transmission electron microscopy and X-ray spectroscopy were composed of mostly carbon and oxygen and internally mixed with nitrogen, sulfur, and potassium (Twohy et al., 2021). Similarly, single-particle mass spectrometry of cloud droplet residuals showed the presence of individual aged biomass burning particles with secondary ammonium, sulfuric acid, oxidized organics, and oxalic acid (Pratt et al., 2010). In addition to chemical composition changes, physical and optical properties of smoke particle changes as smoke plumes age, with particle diameter increasing, and absorption decreasing (Kleinman et al., 2020; Nikonovas et al., 2015).

Within cloud droplets, aqueous reactions can occur and alter cloud droplet chemical composition (Blando & Turpin, 2000; Ervens et al., 2011; Sun et al., 2021). For example, components of biomass burning aerosols (e.g., levoglucosan, catechol, aminophenol) can react with aqueous hydroxyl radicals to form cloud processing tracers, such as oxalate, malonate, and mesoxalate (Tomaz et al., 2018). Levoglucosan, a common molecular tracer in biomass burning particles (Simoneit et al., 1999), has been identified in smoke-influenced cloud water (Desyaterik et al., 2013), and can undergo cloud processing (Tomaz et al., 2018) which causes it to degrade over time (Hennigan et al., 2010). The aqueous lifetime of levoglucosan ranges from a few hours to a few days (Sang et al., 2016; Zhao et al., 2014), depending on temperature, relative humidity, and particle chemical composition (Bai et al., 2013; Lai et al., 2014; Sang et al., 2016; Zhao et al., 2014). Further, smoke-influenced cloud water collected in the Philippines and China showed increased concentrations of organic and light absorbing compounds formed through secondary reactions (Desyaterik et al., 2013; Stahl et al., 2021). Gilardoni et al. (2016) estimated 4%–20% of total organic aerosol measured per year in Europe was formed through aqueous reactions, with the aqueous secondary organic aerosol being more absorbing compared to primary biomass burning organic aerosol.

Lance et al. (2017) recently pointed to the need for observational and modeling studies of cloud processing and the utility of the Whiteface Mountain Observatory in New York. The state of New York frequently experiences high $PM_{2.5}$ concentrations associated with long-range transported smoke (Hung et al., 2021; Rattigan et al., 2016), with increasing elemental and black carbon concentrations in the past two decades (Blanchard et al., 2019). This smoke likely contributes to the organic matter observed in cloud water collected at Whiteface Mountain. At this site, Cook et al. (2017) observed the presence of biomass burning markers resulting from aqueous-phase oxidation reactions of syringol and guaiacol, in three wildfire-influenced cloud water samples collected during August 2014. In another study, cloud water collected during summertime (August 2017) at Whiteface Mountain was found to be primarily composed of organic matter, averaging 66%–78%, by mass, for the non-water components (Zhang et al., 2019). During the same study examining cloud water in August 2017, Lance et al. (2020) observed a correlation between cloud water potassium concentrations and enhancements in black

carbon and ozone concentrations, with air mass trajectory modeling consistent with the influence of long-range transported smoke from wildfires in British Columbia. Together these studies suggest that long-range transported smoke frequently influences clouds at Whiteface Mountain, and this motivates our current work, especially given growing concern of increasing wildfire activity.

The goal of this study is to examine the influence of wildfires on cloud chemical composition at Whiteface Mountain, New York during the summer across 8 years. For the past three decades, cloud water has been collected at the summit of Whiteface Mountain for long-term chemical composition monitoring (Aleksic et al., 2009; Khwaja et al., 1995). In the current study, backward air mass trajectories and satellite-detected smoke were used to determine the frequency with which cloud water samples collected at this site had likely been influenced by smoke. The inorganic ion and total organic carbon concentrations of cloud water samples impacted by smoke were compared to those without smoke influence. A subset of the smoke-influenced cloud water samples was analyzed to further probe the heterogeneity in inorganic ion composition, carbohydrate composition, insoluble residual particle concentrations, and presence of light-absorbing compounds.

2. Materials and Methods

2.1. Whiteface Mountain In Situ Measurements and Cloud Water Collection

Cloud water was collected using an omni-directional passive collector (Aleksic & Dukett, 2010) during June to September from 2010 to 2017 at the Whiteface Mountain Summit Observatory (elevation 1,483 m above mean sea level). Cloud water collection was initiated when the following meteorological parameters were met: (a) liquid water content (LWC) was greater than 0.05 g m^{-3}, indicating the presence of a cloud (Seinfeld & Pandis, 2016), (b) temperature exceeded 2°C, to prevent damage to the collector from riming, (c) no rain was detected, to limit measurements to non-precipitating clouds, and (d) wind speed was greater than 2 m s^{-1}, allowing cloudy air to pass through the collector. LWC was measured by a Gerber Particle Volume Monitor (Gerber, 1991). Wind speed was measured using a RM Young anemometer. Rain was detected using an Aerochem gridded rain sensor from 1994 to 2014; since 2015 rain was detected using a Canadian Acid Precipitation Monitoring Network (CAPMoN) rain sensor (Mekis et al., 2018). Prior to 2014, cloud water was collected in 3 hr intervals. Starting in 2014 this was changed to 12 hr collection intervals. Once collected and labeled, cloud water samples were refrigerated at 4°C for up to 3 days until analysis (Baumgardner et al., 1997; Schwab et al., 2016). In total, 1,338 cloud water samples were collected over 485 days between June and September of 2010–2017. Of those samples, five samples, collected on 16 and 18 August 2014 and 7, 17, and 21 July 2015, were shipped frozen and stored frozen in the dark until further analysis.

Long-term measurements of ozone (O_3), carbon monoxide (CO), nitric oxide (NO), nitrogen dioxide (NO_2), total nitrogen oxides (NO_y), and sulfur dioxide (SO_2) were measured at the Whiteface Mountain Summit Observatory by the University of Albany Atmospheric Sciences Research Center. Method details for the gas measurements can be found in Brandt et al. (2016). Briefly, O_3 was measured using ultraviolet (UV) optical absorption (model 49C, Thermo Environmental Instruments, Inc., Waltham, Massachusetts, USA). CO was measured by non-dispersive infrared coupled with a gas filter correlation (model 300EU, Teledyne API, San Diego, California, USA). NO, NO_2 (after photolytic conversion), and NO_y (after heated molybdenum conversion) were measured using chemiluminescence (model 42CTL, Thermo Environmental Instruments, Inc., Waltham, Massachusetts, USA). SO_2 was measured by pulsed fluorescence (model 43CTL, Thermo Environmental Instruments, Inc., Waltham, Massachusetts, USA).

2.2. Cloud Water Analysis

Samples were analyzed by the Adirondack Lake Survey Corporation (ALSC) for pH, conductivity, LWC, sulfate (SO_4^{2-}), nitrate (NO_3^-), chloride (Cl^-), calcium (Ca^{2+}), magnesium (Mg^{2+}), sodium (Na^+), potassium (K^+), ammonium (NH_4^+), and total organic carbon (TOC). pH was measured using an Orion Star A211 meter with an Orion 8102BNUWP pH probe (Thermo Scientific, Waltham, Massachusetts, USA). Conductivity was measured at 25°C using a YSI Model 32 Conductivity meter with a YSI Model 3,402 probe (Yellow Springs Instrument Co., Yellow Springs, Ohio, USA). TOC was measured according to the EPA 450.1 method using a Tekmar Dorhmann Phoenix 800 Carbon Analyzer (Teledyne Tekmar, Mason, Ohio, USA) from 2010 to 2015. Starting

in April 2015, TOC was measured with a Teledyne Tekmar TOC Fusion Carbon Analyzer (Teledyne Tekmar, Mason, Ohio, USA).

Prior to 2014, the concentrations of SO_4^{2-}, NO_3^-, and Cl^- were measured using a Thermo Scientific Dionex ICS-600 Ion Chromatography system (Thermo Scientific, Waltham, Massachusetts, USA) according to the EPA 300.1 method. After July 2014, the anion concentrations were measured using a Thermo Scientific Dionex ICS-1100 Ion Chromatography system (Thermo Scientific, Waltham, Massachusetts, USA). Thermo Scientific Dionex Ionpac AS22 chromatography columns (Thermo Scientific, Waltham, Massachusetts, USA) were used in both ion chromatography systems. Prior to 2014, the concentrations of Ca^{2+}, Mg^{2+}, Na^+, and K^+ were measured with a Perkin-Elmer AAnalyst (model 300, Perkin-Elmer, Waltham, Massachusetts, USA) flame/graphite furnace Atomic Absorption Spectrometer (AAS). After September 2014, Ca^{2+}, Mg^{2+}, Na^+, and K^+ concentrations were measured with a Perkin-Elmer PinAAcle 900H flame/graphite furnace AAS (Perkin-Elmer, Waltham, Massachusetts, USA). NH_4^+ concentrations were measured using the automated phenolate method combined with colorimetry according to the EPA 350.1 method using a Technicon II AutoAnalyzer (Technicon Industrial Systems, Tarrytown, New York, USA). The limits of detection (LODs) for these inorganic ions were recorded yearly based on 3 times the standard deviation of 7 replicates of a low-level standard and can be accessed on the ALSC website (http://www.adirondacklakessurvey.org/wfc.shtml, last accessed: 28 September 2021). The range of LODs for the years included in this study were 0.05–0.4 μM for SO_4^{2-}, 0.06–0.3 μM for NO_3^-, 0.08–0.5 μM for Cl^-, 0.1–0.7 μM for Ca^{2+}, 0.04–0.1 μM for Mg^{2+}, 0.04–0.7 μM for Na^+, 0.05–0.2 μM for K^+, and 0.8–4 μM for NH_4^+. Any concentration below the LOD for a given sample was replaced with 0.5 multiplied by the LOD for all calculations and figures (MacDougall et al., 1980).

Five cloud water samples collected on 16 and 18 August 2014 and 07, 17, and 21 July 2015 that had sufficient volume remaining after the routine measurements were chosen for additional analyses. The size distributions of insoluble particles were measured for four of the five selected cloud water samples (16 August 2014 and July 07, 17, and 21, 2015) for which sufficient volume remained at the time of analysis. Insoluble particles were measured with an NanoSight LM10 Nanoparticle Tracking Analysis (NTA) Microscope (NanoSight Ltd., Amesbury, UK), which has been previously used for rain water samples (Axson et al., 2015). Briefly, the hydrodynamic diameter of particles, ranging from 20 to 1,000 nm is determined by illuminating the sample using a 405 nm laser diode and tracking individual particles' Brownian motion. All samples were introduced into the sample chamber using a syringe pump set to a speed of 60 rpm. A scientific complementary metal oxide semiconductor (sCMOS) camera collected videos of the light scattering from insoluble particles to measure the number concentrations and size distribution. Each sample was captured 10 times, with 60 s videos. Changes due to thawing frozen samples are not expected to have affected the measured insoluble particle size distributions, based on previous work (Axson et al., 2016).

For the five selected smoke influenced cloud water samples collected between August 2014 and July 2015, high-performance anion-exchange chromatography with pulsed amperometric detection (HPAEC-PAD) was used to measure levoglucosan, mannosan, galactosan, galactose, glucose, mannose, glycerol, inositol, threitol, mannitol, arabinose, and xylose. The analysis was conducted on a Dionex DX-500 ion chromatography system with detection via an ED-50/ED-50A electrochemical cell (Thermo Scientific, Waltham, Massachusetts, USA). A sodium hydroxide gradient was used on a Dionex CarboPac PA-1 column (4 × 250 mm). The complete run time was 50 min with an injection volume of 100 μL. Full method details are reported by Sullivan, Frank, Kenski, et al. (2011), Sullivan, Frank, Onstad, et al. (2011), and Sullivan et al, (2014, 2014). The LODs were determined to be less than 0.01 μg L^{-1} for all carbohydrates measured. The organic acids acetate, proponiate, formate, methanesulfonate, glutarate, succinate, malonate, maleate, and oxalate were measured using a Dionex ICS-4000 capillary ion chromatography system (Thermo Scientific, Waltham, Massachusetts, USA). A Dionex AS11-HC capillary column (Thermo Scientific, Waltham, Massachusetts, USA) with a potassium hydroxide gradient provided by an eluent generator at a flowrate of 0.015 mL min^{-1} was used for the separation. The complete run time was 65 min with an injection volume of 35 μL. The LODs was determined to be less than 0.1 μg L^{-1} for all organic acid species measured. Uncertainty for all carbohydrate and organic acid species measured were calculated by propagating error and estimated to be ∼10% of the measured concentration.

For two of the selected smoke influenced cloud water samples (collected on 7 and 17 July 2015) for which sufficient sample remained, ultraviolet (UV)-visible light absorption spectra were measured with a 1-m optical path capillary waveguide (WPI LWCC 3100), a deuterium-tungsten lamp (Ocean Insight DH-mini, Ocean Insight,

Orlando, Florida, USA), and a modular spectrometer (Ocean Optics USB4000, Ocean Insight, Orlando, Florida, USA). Absorption spectra were recorded between 300 and 600 nm. Cloud water was filtered with a 0.2 μm syringe filter prior to analysis to prevent insoluble particles from obstructing the capillary waveguide. Each spectrum was baseline corrected by subtracting the absorbance in the near IR (700 nm), following the approach described by Hecobian et al. (2010) and Zhang et al. (2011). Each absorbance measurement included at least four replicates, and the absorbance uncertainty was determined by the standard deviation of those measurements at each wavelength. Water-soluble organic carbon (WSOC) was measured in triplicate for these two cloud water samples using a Sievers 5310C Laboratory TOC (GE Analytical Instruments, Boulder, Colorado, USA). The relative standard deviation was less than 1% for each TOC reading. Mass absorption coefficients (MAC) were calculated following the equation below.

$$\mathrm{MAC}_{\mathrm{Cloud\ Water}} = \frac{\mathrm{Abs}_{365}}{(1\ \mathrm{m})\left(\mathrm{WSOC}_{\mathrm{ppm}}\right)} \tag{1}$$

where Abs_{365} refers to the absorbance averaged between 360 and 370 nm, 1 m refers to the length of the optical path capillary waveguide, and $\mathrm{WSOC}_{\mathrm{ppm}}$ is the water-soluble organic carbon concentration in units of ppm.

The absorption Ångström exponent (AAE) was calculated to probe the wavelength (λ) dependence of aerosol absorptivity in the cloud water samples using the following relation (Bian et al., 2020; Kirillova et al., 2014):

$$\mathrm{AAE} = -\frac{\ln(A(\lambda_1)) - \ln(A(\lambda_2))}{\ln(\lambda_1) - \ln(\lambda_2)} \tag{2}$$

where $A(\lambda)$ denotes the cloud water absorptivity at a particular wavelength (λ). AAE was determined within the range of 330 (λ_1)–400 (λ_2) nm to avoid interferences from non-organic compounds such as nitrates at ∼300 nm (Cheng et al., 2011) and due to the low signal-to-noise ratio for wavelengths above 400 nm as similarly observed in previous studies (Kirillova et al., 2014).

2.3. Air Mass Trajectory Analysis

For each cloud water sample collected between June and September of 2010–2017, a 3 day (72 hr) backward air mass trajectory was calculated using the NOAA Hybrid Single Particle Lagrangian Integrated Trajectory (HYSPLIT) Model (Rolph et al., 2017; Stein et al., 2015). The midpoint of the cloud water collection period was used as the start time for the backward air mass trajectory. To account for uncertainties in the HYSPLIT model related to local terrain, a starting height at 1,583 m above sea level (100 m above the sampling site at 44.366°N, 73.903°W) was used. Trajectories were calculated using 1° Global Data Assimilation System (GDAS) meteorology.

The NOAA Hazard Mapping System (HMS) Fire and Smoke Product (Rolph et al., 2009) was used to ascertain whether cloud water collected may have been influenced by smoke. Previous studies have similarly used the HMS Fire and Smoke Product to differentiate smoke influenced days (Brey, Ruminski, et al., 2018; O'Dell et al., 2019). The HMS Fire and Smoke Product incorporates multiple satellite operations to identify locations of fire and smoke across North America. The HMS smoke location and classifications are identified manually, and therefore, the product can include errors when distinguishing smoke and other features (e.g., clouds, forests, and bodies of water) that appear similarly in satellite imagery (Schroeder et al., 2008). The HMS does not distinguish between different sources of smoke (e.g., wildfires, prescribed burns) and is limited to smoke visible during daylight hours (Brey, Barnes, et al., 2018; Brey, Ruminski, et al., 2018).

The HMS Fire and Smoke Product was used in conjunction with the modeled backward air mass trajectories to classify the influence of biomass burning for each day cloud water samples were collected. These cloud water samples were then sorted into three categories based on their probability of having smoke influence: (a) satellite-detected smoke influencing air quality over Whiteface Mountain, (b) satellite-detected smoke observed along the backward air mass trajectory, and (c) no satellite-detected smoke influence. The first category (referred to as having a high probability of smoke influence) included any day when the first 12 hr of the backward air mass trajectory overlapped with any identified smoke, regardless of smoke thickness. The second category (referred to as having a moderate probability of smoke influence) encompassed days for which the latter portion of the backward air mass trajectory (13–72 hr before arrival at Whiteface Mountain) overlapped with

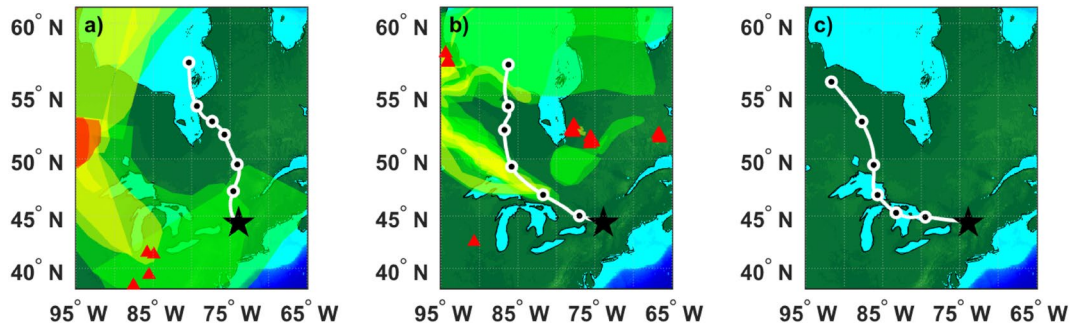

Figure 1. Smoke classifications for Whiteface Mountain cloud water samples. NOAA HYSPLIT 72 hr backward air mass trajectories (white lines, with black dots representing every 12 hr resolution) are overlaid on smoke maps, where green, yellow, and red shading indicates thin, medium, and thick amounts of smoke, respectively, as defined by the NOAA Hazard Mapping System (HMS) Fire and Smoke Product. Red triangles indicate locations of satellite-detected wildfires. Samples were classified by the probability of being smoke-influenced with "high probability" (a) if the HMS displayed smoke above Whiteface Mountain or within the first 12 hr of the backward air mass trajectory, "moderate probability" (b) if the air mass trajectory between 13 and 72 hr overlapped with the smoke map, and "low probability" (c) if the trajectory did not overlap with any smoke detected.

satellite-observed smoke. The third category (low probability of smoke influence) corresponded to samples for which no satellite-observed smoke overlapped with the traveling air mass. Uncertainties in the air mass trajectories were considered by creating a radius starting at zero and expanding by 2 km for every hour along the trajectory; this area corresponded to the region for which HMS Fire and Smoke product overlap was considered. Lastly, partial backward air mass trajectories that encountered precipitation during 13–72 hr were not considered in the classification due to wet deposition potentially impacting the air mass and removing smoke particles. Since cloud water was not collected during rainfall (Section 2.1), any precipitation reported by the HYSPLIT model within the first 12 hr of the air mass trajectory was not considered. Wet deposition effects have been observed in previous studies at this site showing a coincident drop in ion concentrations in cloud water collected after rain showers (Aleksic et al., 2009; Khwaja et al., 1995). Figure 1 shows the backward air mass trajectories overlaid on HMS smoke and fire maps for three example cloud water samples representing each of the smoke categories.

3. Results and Discussion

3.1. Frequency of Wildfire Smoke Plumes Influencing Whiteface Mountain

Cloud water samples were collected at 3 or 12 hr intervals, depending on the collection year, for 485 days between the months of June and September from 2010 to 2017, resulting in a total of 1,338 samples included in this analysis. Based on backward air mass trajectory analysis, the Whiteface Mountain Observatory was primarily influenced by smoke from fires occurring in Canada and the eastern United States (e.g., Figures 1 and S1 in Supporting Information S1), consistent with previous observations of long-range transported smoke impacting air quality in New York State (Brey, Ruminski, et al., 2018; DeBell et al., 2004; Park et al., 2007; Rogers et al., 2020; Wu et al., 2018).

Of the 485 days when cloud water was sampled in this study, 49 ± 3% of these days were identified as having a moderate to high probability of smoke influence. Of the days with smoke influence, 29 ± 2% were classified as "high smoke probability," meaning that smoke was detected by the NOAA HMS Fire and Smoke Product over Whiteface Mountain, while 20 ± 2% of the days were influenced by upwind smoke along the trajectory (designated as "moderate smoke probability" samples). Cloud water collected from June through August were more likely to be smoke-influenced (51 ± 6%, 59 ± 6%, and 48 ± 5%, respectively), compared to cloud water collected in September (34 ± 5%) (Figure 2a), with uncertainties representing standard errors assuming binomial distributions. Within the contiguous United States fire season differs regionally with fires in the western United States occurring through the summer to fall months (June–November), central states beginning in the spring to summer months (April–July), and the southern states throughout the fall (September–December) and winter months (January–March) (Jaffe et al., 2020). The increase in smoke-influenced cloud water during June and July correspond to when satellite-detected fires begin to peak in the western United States and in some of the Canadian

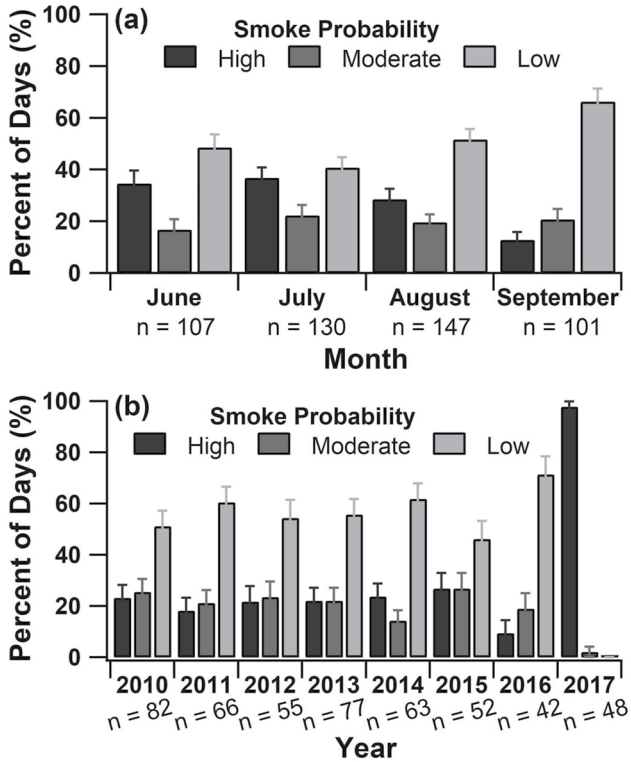

Figure 2. Frequency of smoke influence on cloud water collected at Whiteface Mountain, New York. Percentage of days classified by their smoke influence by month between 2010 and 2017 (a) and by year considering the months of June to September (b). The number (n) of cloud water samples per month (a) and per year (b) are denoted under each category. Error bars represent standard errors in frequency percentages and were calculated assuming binomial distributions.

provinces (Brey, Ruminski, et al., 2018; Liu et al., 2010). Generally, there are few local wildfires in the northeastern United States; however, degradation of air quality in the northeastern states is prevalent during the summer months (July–September) when transported smoke-attributable total carbonaceous aerosol and $PM_{2.5}$ levels peak (O'Dell et al., 2021; Park et al., 2007).

Over the 8-year period studied, the frequency of smoke-influenced days did not significantly change between 2010 and 2015 (Figure 2b). 45 ± 2% of the days when cloud water was sampled between 2010 and 2015 were classified as having had smoke influence. The summer of 2016 had a significantly lower (t-test, $p < 0.05$) percentage of smoke-influenced days (29 ± 2%) compared to the previous years in this study (Figure 2b). During 2016 compared to the 2015 and 2017 summer seasons, Jaffe et al. (2020) reported lower total United States wildfire area burned, and O'Dell et al. (2021) reported lower smoke-attributable asthma emergency visits in the northeastern United States. Similarly, total number of fires and area burned in Canada was lower in 2016 compared to the 2015 and 2017 wildfire season (Tymstra et al., 2020). All cloud water samples collected in 2017 ($n = 48$) were smoke-influenced, consistent with previous analysis showing elevated ozone, black carbon, and cloud water potassium concentrations during August 2017 at Whiteface Mountain (Lance et al., 2020). Additionally, $PM_{2.5}$ concentrations were greater in 2017 for the western United States than in the previous decade (Xie et al., 2020) due to extreme wildfire conditions in these states (Jaffe et al., 2020) and Canada (Matz et al., 2020). During these large fire events, a substantial decline in air quality was observed throughout the United States (Jaffe et al., 2020), consistent with the increase in smoke-influenced cloud water observed here for 2017.

3.2. Cloud Water Composition During Smoke Influence

Cloud water inorganic ion concentrations, LWC, pH, and TOC concentrations, as well as trace gas levels, were evaluated for differences among the smoke classifications using the Kruskal-Wallis non-parametric test and Dunn's post hoc pairwise comparison test, with the level of significance set at $p < 0.05$ (95% confidence interval). The Kruskal-Wallis statistical test was used to evaluate differences in the distributions between the three smoke classifications, because the data observed were non-normally distributed. The non-normal distributions were mainly due to samples containing low ion concentrations, as shown in the boxplot distributions in Figures 3 and S2 in Supporting Information S1. Significant differences between the smoke classifications (high vs. low smoke probability and moderate vs. low smoke probability) were observed for all measured inorganic ion concentrations (SO_4^{2-}, NO_3^-, Cl^-, Ca^{2+}, Mg^{2+}, Na^+, K^+, NH_4^+) and TOC concentrations, as well as CO and O_3 concentrations (Figures 3, S2, and S3, Table S1 in Supporting Information S1). In addition, significant differences in the distributions for SO_2 and NO concentrations were observed between the high and low smoke influence probabilities (Figure S3 in Supporting Information S1). For LWC, there was a significant difference in the distribution between the moderate smoke probability category compared to the high and low smoke probability categories, but no trend was observed between all three categories. The 8-year summertime average for LWC in this study was similar to the 1994–1999 mean LWC at Whiteface Mountain (0.57 g m^{-3} (Baumgardner et al., 2003)). The lack of trend between the LWC distributions supports the observed differences in inorganic ion concentrations between the three smoke classifications not being caused by LWC differences (Aleksic & Dukett, 2010; Khwaja et al., 1995; Li et al., 2020).

The pH distributions between the smoke categories were not statistically different and displayed similar median and range of pH values (Table S1 in Supporting Information S1). The mean pH values (with the 95% confidence intervals) for the high, moderate, and low smoke probability categories were 4.69 ± 0.06, 4.68 ± 0.08, and 4.72 ± 0.04, respectively. Cloud water mean pH values at this site have steadily climbed from pH 4.0 to 4.7 since measurements began in 1994 (Aleksic et al., 2009; Falconer & Falconer, 1980; Khwaja et al., 1995; Schwab

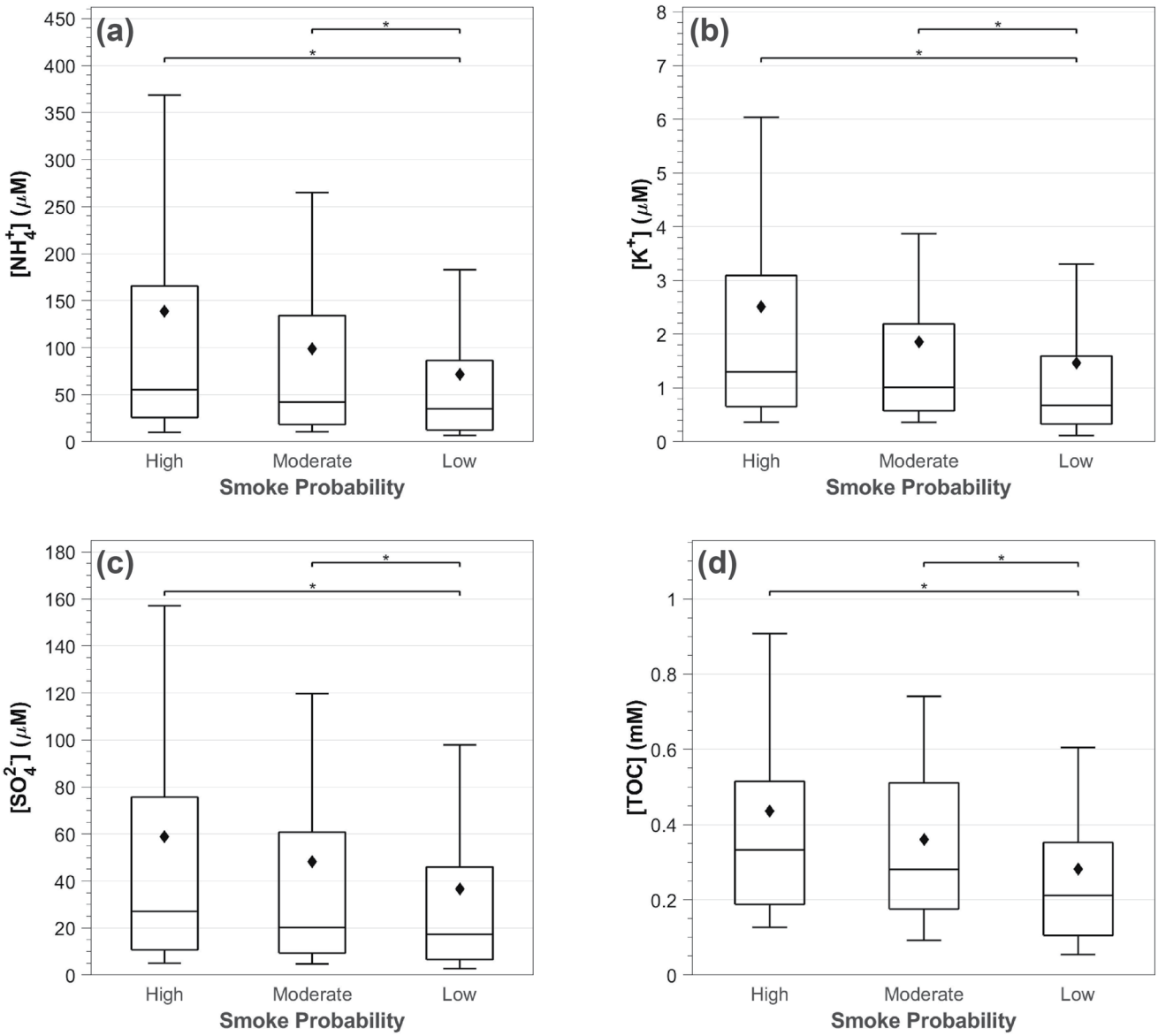

Figure 3. Boxplot distributions for (a) potassium (K^+), (b) ammonium (NH_4^+), (c) sulfate (SO_4^{2-}), and (d) total organic carbon (TOC) concentrations per category of smoke influence probability (high, moderate, and low). Boxplots represent the 25th, 50th, and 75th percentiles, with whiskers representing the 10th and 90th percentiles. Average concentrations per smoke category are marked as diamonds. Significant differences in the distributions that met both the Kruskal-Wallis non-parametric and Dunn's post hoc pairwise comparison tests ($p < 0.05$) are annotated with an asterisk above the box plots.

et al., 2016); this increase is attributed to decreases in SO_2 and NO_x emissions in the recent decades (Schwab et al., 2016).

Cloud water with a high probability of smoke influence had greater median and mean inorganic ion concentrations compared to cloud water with a low probability of smoke influence, for SO_4^{2-}, NO_3^-, Cl^-, Ca^{2+}, Mg^{2+}, Na^+, K^+, and NH_4^+ (Figures 3, S2, and Table S1 in Supporting Information S1). Cloud water TOC followed the same trend patterns to the inorganic ions measured (Figure 3 and Table S1 in Supporting Information S1). Previously, in southeast Asia, K^+, NH_4^+, SO_4^{2-}, and TOC were associated with biomass burning influence in cloud water (Stahl et al., 2021). Similarly, Figure 3 shows boxplot distributions of K^+, NH_4^+, SO_4^{2-}, and TOC with significant differences in their distributions, as determined by the Kruskal-Wallis statistical test ($p < 0.05$, Table S1 in Supporting Information S1) for the high smoke probability compared to the low smoke probability, as discussed below.

The mean potassium (K^+) cloud water concentrations (with the 95% confidence intervals) during the high, moderate, and low smoke probability conditions were 2.5 ± 0.4, 1.9 ± 0.4, and 1.5 ± 0.2 μM, respectively (Figure 3a). The 10th and 90th percentiles of the potassium concentrations for cloud water samples classified as having a high smoke probability were 0.4 and 6.0 μM, respectively, compared to 0.1 and 3.3 μM, respectively, for the samples with a low probability of smoke influence, further illustrating the impact of smoke influence on the cloud water. The mean potassium concentration for the high smoke probability category was also greater than the summertime mean measured at Whiteface Mountain from 1994 to 2006, with the exception of 2003, which was characterized by higher concentrations of the majority of the measured ions, compared to the surrounding years (Aleksic et al., 2009). The increase potassium concentrations in cloud water for samples with a high probability of smoke influence is expected, since potassium is an inorganic smoke marker that has been noted in previous cloud water samples impacted by wildfire events (Cook et al., 2017; Stahl et al., 2021). Additional variations in potassium concentration can also be due to mineral dust and agricultural sources (Straub et al., 2012).

Ammonium (NH_4^+) and sulfate (SO_4^{2-}) mean concentrations (with the 95% confidence intervals) were approximately double for the high smoke probability category and ~1.6 times greater for the moderate smoke probability category compared to the low smoke probability category (140 ± 20 and 59 ± 8 μM for high smoke probability samples, 100 ± 20 and 48 ± 10 μM for moderate smoke probability samples, compared to 72 ± 7 and 37 ± 3 μM for low smoke probability samples, respectively) (Figure 3 and Table S1 in Supporting Information S1). Historically, ammonium and sulfate have been the dominant inorganic ion species measured in cloud water at Whiteface Mountain and have been associated with air masses originating from polluted areas, especially from the Midwest United States (Aleksic et al., 2009; Khwaja et al., 1995; Schwab et al., 2016). Further, ammonium and sulfate-containing particles have been associated with biomass burning emissions (Zhou et al., 2017), and observed in aged biomass burning particles (Pratt et al., 2010). The ammonium and sulfate cloud water concentrations for the high smoke probability category were within the same range as smoke-influenced cloud water at a site in Southeast Asia (Stahl et al., 2021), but previous studies have noted that ammonium and sulfate concentrations vary widely depending on meteorological conditions and regional influences (Hutchings et al., 2009; Schwab et al., 2016). While the high and moderate smoke probability categories had similar tenth percentile concentrations of ammonium (both 10 μM) and sulfate (both 5 μM), compared to the low smoke probability category (7 and 3 μM, respectively), they were characterized by higher 90th percentiles of ammonium (~300 μM for high and moderate smoke probability categories compared to ~200 μM for the low smoke probability category), and SO_4^{2-} (157, 120, and 98 μM for high, moderate, and low smoke probability categories, respectively) (Figure 3). This further shows that even with varying regional and meteorological conditions, air masses that are mixed with smoke display increased cloud water concentrations of ammonium and sulfate, on average.

TOC concentrations were also significantly higher for cloud water classified as having a high smoke probability at Whiteface Mountain, compared to the low smoke probability (Figure 3d). The mean TOC concentrations (with the 95% confidence intervals) for the high, moderate, and low smoke probability categories were 0.44 ± 0.05, 0.36 ± 0.05, and 0.28 ± 0.02 mM, respectively. These average concentrations are in the range of previously reported wildfire-influenced TOC concentrations in fog and cloud water in the United States (0.08–1 mM) (Stahl et al., 2021 and references therein). Further, the 90th percentile TOC concentrations increased between smoke categories (0.60, 0.74, and 0.91 mM for the low, moderate, and high smoke probabilities, respectively). Note that TOC can be enhanced for reasons other than primary smoke influence, including anthropogenic influence (Herckes et al., 2013; Kawamura & Gagosian, 1987) and aqueous-phase secondary organic aerosol production in clouds (Blando & Turpin, 2000; Chen et al., 2015; Gilardoni et al., 2016; Lee et al., 2012; Yuan et al., 2004).

Significant differences in the distributions of O_3, CO, SO_2, and NO levels between the smoke conditions were observed at the summit of Whiteface Mountain (Figure S3 in Supporting Information S1). O_3, CO, and SO_2 levels increased with increasing smoke probability, whereas NO decreased with increasing smoke probability (low, moderate, and high). Both O_3 and CO have been associated with long-range transported smoke that impacted air quality hundreds of km away from the fire source (Briggs et al., 2017; Dreessen et al., 2016; Rogers et al., 2020). O_3 is an important atmospheric oxidant that is often produced in smoke plumes during the daytime (Akagi et al., 2013). CO is produced during flaming combustion and is commonly used to identify smoke plumes (Liu et al., 2017; Urbanski, 2013). SO_2 is produced from anthropogenic and biomass burning emissions (Chuang et al., 2016) and is oxidized to form sulfate, which can participate in brown carbon production in the aqueous phase (De Haan et al., 2020). NO rapidly reacts in wildfire plumes to produce nitroaromatic compounds

Table 1
Summary of Smoke Probability Classifications, Sampling Start Times, Inorganic Ion Concentrations, pH, and TOC Concentrations for Selected Cloud Water Samples Collected at the Whiteface Mountain Observatory

Sample ID	Smoke probability	Sampling start time	SO_4^{2-} (μM)	NO_3^- (μM)	Cl^- (μM)	Ca^{2+} (μM)	Mg^{2+} (μM)	Na^+ (μM)	K^+ (μM)	NH_4^+ (μM)	pH	TOC (mM)
C1	High	07/07/2015 18:00	65.7	37.4	3.0	9.1	3.4	3.7	3.7	125.3	4.4	0.6
C2	High	08/16/2014 18:00	4.6	4.9	0.3	1.6	0.8	bdl	0.4	7.6	5.2	0.1
C3	High	08/18/2014 06:00	8.6	6.2	8.5	0.7	1.2	7.8	1.1	12.9	4.8	0.2
C4	Low	07/17/2015 18:00	19.3	19.5	1.5	6.7	1.9	1.5	0.5	43.4	4.7	0.2
C5	Low	07/21/2015 18:00	5.5	7.8	0.8	7.1	1.7	0.9	0.5	24.4	5.5	0.3

Note. Values below the limits of detection are marked as "bdl." All samples were collected over a 12 hr integration period.

(Becidan et al., 2007; Peng et al., 2021; Selimovic et al., 2020), and anthropogenic sources of NO can mix with smoke plumes to increase O_3 levels (Jacob et al., 2010). Together, these trace gas trends give greater confidence to the smoke classification used in this study and further show the influence of the transport of wildfire smoke on air quality.

3.3. Case Studies: Smoke-Influenced Cloud Water Composition

Five smoke-influenced cloud water samples were selected for additional chemical and physical analyses to further examine cloud water composition with smoke influence. While three of these samples (C1, C2, C3) were classified as having a high probability of smoke influence and two samples (C4, C5) having a low probability of smoke influence (Figure S1 in Supporting Information S1), their chemical composition varied, with differences in: (a) inorganic ion concentrations, (b) dissolved organic carbon composition, (c) insoluble particle size distributions and concentrations, and (d) UV-visible absorbance. The air masses for samples C1 and C4 traveled from the southerly direction. Sample C1 was impacted by smoke originating in the southeastern United States, whereas sample C4 did not have any influence from satellite detected smoke. Sample C2 crossed over the Midwest United States and was influenced by fires in the Northwest Territories, Canada. Samples C3 and C5 had air masses originating from the north crossing over or near Hudson Bay, Canada. C3 was influenced by regional smoke over Ottawa, Canada and New York State. Though Figure S1 in Supporting Information S1 shows the air mass trajectory for sample C5 intersecting with the satellite-detected smoke map, this sample encountered precipitation after the twelfth hour along the backward air mass trajectory; thus the 13–72 hr of the air mass were not considered in the classification, as described in Section 2.3. Of the five samples, samples C1 and C4 were also influenced by urban emissions, since the air masses dipped below the modeled mixed (boundary) layer depth (MLD) near several cities (population >50,000), including Columbus, Ohio for C1 and Washington, D.C. for C4. The air mass for sample C2 also spent time in the atmospheric boundary layer, but did not pass by any city with a population greater than 50,000. The air masses for the other two case samples (C3 and C5) traveled primarily above the modeled MLD (Table S2 in Supporting Information S1).

3.3.1. Inorganic Ion and TOC Concentrations

Table 1 lists the case samples' collection dates, smoke classifications, inorganic ion concentrations, pH values, and TOC concentrations. Samples C1, C2, and C3 were classified as having a high probability of smoke influence, but had varying concentrations of inorganic ions. Sulfate, ammonium, potassium, and TOC concentrations for sample C1 were near or greater than the medians for the samples classified as having a high probability of smoke influence, as shown in Figure 3. The C1 sample's backward air mass trajectory traveled below the MLD above urban areas before reaching the sampling site, and this urban influence likely also increased the inorganic ion concentration (Hecobian et al., 2011; Straub et al., 2012). Sample C2 had all measured inorganic ion and TOC concentrations below the 25th percentile for the high probability smoke influence category. While the backward air mass trajectory overlapped with the satellite-detected smoke 2 hr before reaching the sampling site, classifying the sample as having a high probability of smoke influence, it is possible that the air mass influencing the cloud water at Whiteface Mountain did not intercept the smoke based on the low TOC, K^+, NH_4^+, and SO_4^{2-} concentrations. The lack of vertical resolution of the HMS fire and smoke product may account for lower inorganic

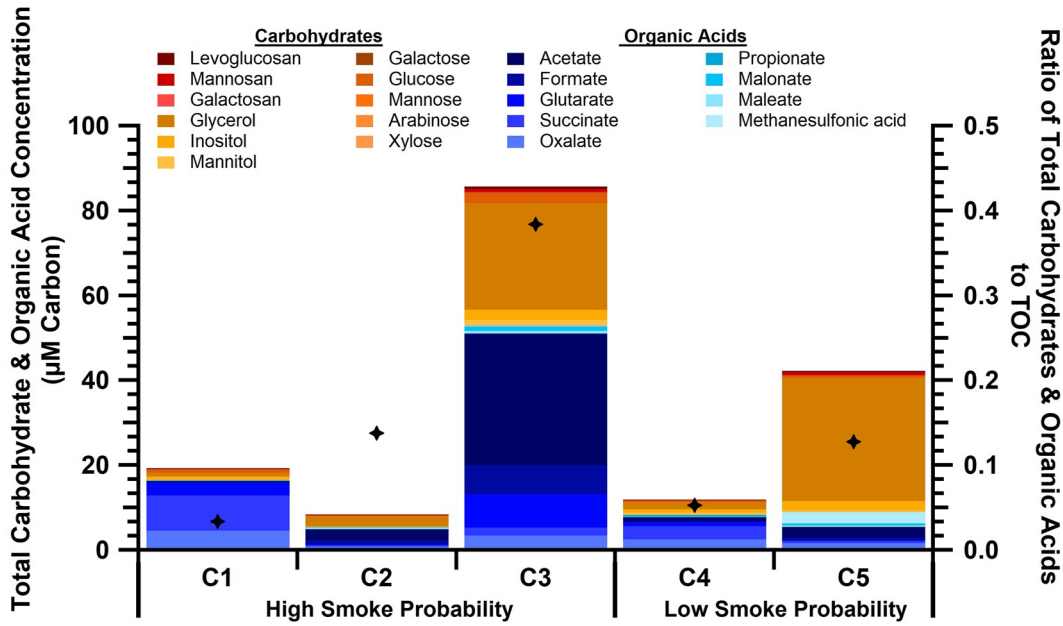

Figure 4. Contributions of carbohydrates measured by HPAEC-PAD and organic acids measured by ion chromatography (left axis) for the five cloud water case samples. Diamond markers represent the ratio of the sum of the carbohydrates and organic acids to the total organic carbon (TOC) concentrations (right axis). Samples C1, C2, and C3 were classified as having a high probability of smoke influence, while samples C4 and C5 were classified as having a low probability of smoke influence.

ion concentrations compared to its smoke category, as the air mass altitude may not have intersected the smoke altitude. Sample C3 had lower inorganic ion concentrations (between the 10th and 50th percentiles) compared to samples with a high probability of smoke, except for chloride (Cl^-) and (Na^+), potentially sourced from sea spray aerosol from Hudson Bay (May et al., 2018). Samples C4 and C5 were classified as having a low probability of smoke influence. Sample C4 had all inorganic ion concentrations between the 25th and 50th percentiles for the low smoke probability category. Sample C5 had inorganic ion concentrations below or near the median for low smoke probability samples. The air mass for sample C5 primarily stayed above the MLD and encountered precipitation during transport, likely contributing to the low inorganic ion concentrations observed.

3.3.2. Dissolved Organic Carbon Composition

Concentrations of smoke-related organic compounds (levoglucosan, mannosan, and galactosan, measured by HPAEC-PAD, and oxalate, measured by ion chromatography) were used to further examine biomass burning influence. Concentrations of other relevant organic carbon compounds are listed in Table S3 in Supporting Information S1. Figure 4 shows the concentrations of measured carbohydrates and organic acids, as well as the ratio of all measured organic carbon compounds relative to the measured TOC concentration (Table 1). This ratio was highest for sample C3 (0.38 ± 0.03). Sample C3 was classified as having a high probability of smoke influence, with fire hotspots identified by the HMS Smoke and Fire product near New York State and Ottawa, ON, Canada. Despite having lower inorganic ion concentrations (Table 1), sample C3 was characterized by an air mass that remained above the MLD, suggesting in-cloud dissolution and production of organic compounds, as evident by carboxylic acids (acetate, formate, glutarate, succinate, and oxalate) contributing to 60% of the measured organic compounds (Figure 4). Samples C1 and C4 had the lowest amounts of measured carbohydrates relative to the measured TOC (0.03 and 0.05, respectively), suggesting greater OC influence from non-smoke sources, including urban emissions, consistent with the backward air mass trajectory dipping below the MLD less than 1 day before reaching the sampling site. All five cloud water case samples had measurable concentrations of levoglucosan (0.02–0.09 μM, Table S3 in Supporting Information S1), which is a common smoke aerosol tracer (Fabbri et al., 2009; Simoneit et al., 1999; Sullivan et al., 2011a) produced from the pyrolysis of wood during biomass burning. Concentrations of mannosan and galactosan, isomers of levoglucosan that are also released during biomass burning events (Engling et al., 2009; Fabbri et al., 2009; Gao et al., 2003; Urban et al., 2014),

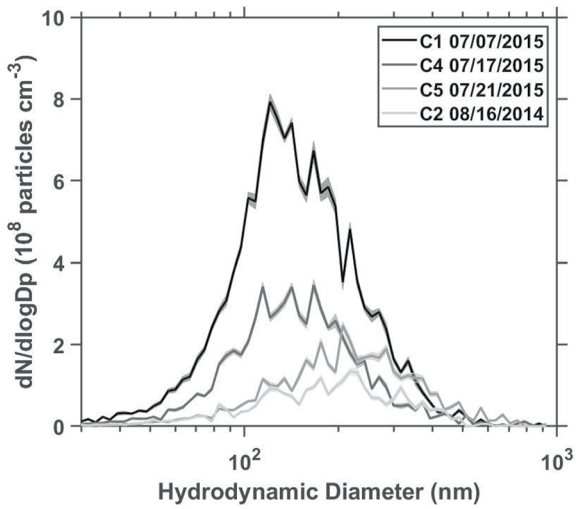

Figure 5. Average insoluble residual particle size distributions for four smoke-influenced cloud water samples with standard deviations shaded.

ranged from 0.12 to 0.74 μM, respectively (Table S3 in Supporting Information S1). No trends in levoglucosan, mannosan, and galactosan concentrations were observed between the smoke categories. However, samples C1 (high smoke probability) and C4 (low smoke probability), which both had their air masses mix below the modeled MLD, did not have detectable concentrations of mannosan and only contained 0.04 μM levoglucosan. Yet, sample C1 featured the highest potassium concentration of the case samples (Table S3 in Supporting Information S1), supporting smoke influence (Section 3.3.1). However, levoglucosan degrades during atmospheric transport (Bai et al., 2013; Hennigan et al., 2010; Hoffmann et al., 2010; Tomaz et al., 2018; Yang et al., 2020; Zhao et al., 2014), which may have reduced levoglucosan concentrations.

To examine the influence of cloud processing on the cloud water case samples, oxalate concentrations were compared between the cloud water case samples. All 5 case samples had oxalate as one of its most abundant measured organic acids. The presence of oxalate is linked to cloud processing due to its aqueous formation mechanism (Ervens et al., 2004; Li et al., 2020; Sorooshian et al., 2013, 2015). Mass ratios of oxalate:sulfate in cloud droplet residual particles have been observed between 0.01 and 0.23, with larger ratios associated with aqueous phase processing occurring at higher cloud altitudes (Hilario et al., 2021; Wonaschuetz et al., 2012). Air masses for samples C2, C3, and C5 spent time aloft (Table S2 in Supporting Information S1), allowing more time for particles to chemically process in the aqueous-phase, resulting in larger oxalate:sulfate ratios (0.08–0.18; Tables 1 and S3 in Supporting Information S1), compared to samples C1 and C4 (0.04 and 0.06, respectively) which spent more time within the MLD. Additional discussion on the cloud processing markers succinate, formate, acetate, and methanesulfonate is included in Supporting Information S1.

3.3.3. Insoluble Residual Particle Concentrations

Soluble components of CCN can dissolve in cloud droplets (Chan et al., 2008; Petters, Carrico, et al., 2009), but not all CCN material is soluble (McFiggans et al., 2006). For example, fresh biomass burning particles can contain poorly soluble organic and black carbon internally mixed with soluble potassium salts (Reid et al., 2005). Further, insoluble soot released from biomass burning is generally a poor CCN (Aquila et al., 2011; Giebl et al., 2002), but can become CCN active as secondary species (e.g., ammonium sulfate and ammonium nitrate) condense onto insoluble particles creating a soluble coating (Aquila et al., 2011; Ervens et al., 2010; Furutani et al., 2008; Khalizov et al., 2009; Leskinen et al., 2007; Petzold et al., 2005). Previous cloud and fog water studies suggest 77%–94% of TOC is soluble, with uptake of soluble compounds (e.g., carboxylic acids and carbonyls) contributing to higher soluble organic carbon fractions (Gioda et al., 2008; Herckes et al., 2013; Paulot et al., 2011; Yu, 2000). To our knowledge, this is the first study to measure the size distributions of insoluble residual particles in cloud water.

Figure 5 shows the submicron size distributions for the insoluble cloud water residual particles in the four smoke-influenced samples measured with NTA. Samples C2 and C5 had smaller particle concentrations (0.60 ($\pm$0.03) $\times$ 10^8 particles mL^{-1} and 1.01 ($\pm$0.04) $\times$ 10^8 particles mL^{-1}, respectively) with larger average mode diameters (185 $\pm$ 14 and 247 $\pm$ 20 nm, respectively). Samples C2 and C5 were characterized by air masses that primarily stayed above the MLD before arriving to the sampling site, likely contributing to the lower insoluble particle concentrations, since aerosol number concentrations in the free troposphere are lower than within the boundary layer (Seinfeld & Pandis, 2016).

Sample C1, which had both smoke and urban influence, contained the highest insoluble particle concentration (3.3 ($\pm$0.2 $\times$ 10^8 particles mL^{-1}) with the smallest mode diameter (135 $\pm$ 6 nm) (Table S2 in Supporting Information S1), consistent with previously analyzed rainwater and melted snow samples that had urban influences (Axson et al., 2015). Sample C4, which had part of its air mass mix below the MLD near Washington, D.C., contained the second highest insoluble particle concentration (1.49 ($\pm$0.06) $\times$ 10^8 particles mL^{-1}) and the second smallest mode diameter (142 $\pm$ 9 nm). These results suggest the urban air masses influencing sample C1 and C4 contained insoluble material made of smaller and less aged particles with lower hygroscopicity. The

higher insoluble particle concentrations for sample C1 and C4 reflect the greater boundary layer influence, with likely contributions from biomass burning (Li, 2019; Petters, Carrico, et al., 2009), and anthropogenic emissions (Ervens et al., 2010; Hudson, 1991; Roberts et al., 2006).

To further highlight the smoke and urban influences on cloud water composition, UV-visible absorbance spectra between 300 and 600 nm were measured for samples C1 and C4, showing decreasing absorptivity with increasing wavelength (Figure S4 in Supporting Information S1). The mass absorption coefficient averaged between 360 and 370 nm (MAC_{365}) and AAE values were calculated to investigate the presence of radiation absorbing compounds in these cloud water samples at Whiteface Mountain. The calculated MAC_{365} values for C1 and C4 were 0.046 ± 0.001 and 0.061 ± 0.001 $m^2\ g^{-1}$, respectively (Table S2 in Supporting Information S1). These values are two to 10 times lower than absorbance measurements of biomass burning organic aerosols extracted from filter samples (Di Lorenzo et al., 2017; Gilardoni et al., 2020; Srinivas & Sarin, 2013) and online measurements from a Particle-Into-Liquid Sampler (Hecobian et al., 2010; Zhang et al., 2011). The corresponding AAE values for samples C1 and C4 were 9 and 8, respectively. The cloud water AAE values were most similar to particle samples with biomass burning influences collected near India (9 ± 3, Srinivas and Sarin (2013)) and in the southeastern United States (∼7 ± 1, Hecobian et al. (2010)). While only two cloud water samples had sufficient volume to measure absorptivity, the MAC_{365} and AAE values support the presence of brown carbon absorbing compounds in the cloud water.

4. Conclusions

In this multiyear (2010–2017) study, 1,338 cloud water samples were collected in the summer months of June to September at Whiteface Mountain, New York. To classify cloud water samples by the probability of smoke influence, 72 hr backward air mass trajectories were modeled for each sample and compared to satellite-derived smoke maps. Of the 485 days when cloud water was collected, 49 ± 3% were classified as having a moderate to high probability of smoke influence. Cloud water samples collected from June through August were more likely to be smoke-influenced (51 ± 6%, 59 ± 6%, and 48 ± 5%, respectively) compared to cloud water collected in September (34 ± 5%). The frequency of smoke-influenced cloud water was lower in years that had fewer wildfires (e.g., 2016) compared to years that had increased wildfire activity (e.g., 2017). It is likely that smoke influence on cloud water will increase in future years as wildfires increase in frequency and severity (Jolly et al., 2015; McClure & Jaffe, 2018; O'Dell et al., 2019). Thus it is imperative that future studies investigate how wildfire smoke impacts aerosol-cloud interactions.

Relying on modeled air mass trajectories and satellite-derived smoke maps to determine smoke influence has inherent uncertainties that may misclassify air masses and cloud water samples. The classification system for differentiating the probability of smoke influence relied on the HMS Fire and Smoke Product, which only provides the horizontal spatial mapping of smoke plumes without identifying the age or altitude of smoke plumes (Brey, Ruminski, et al., 2018). In addition, backward air mass trajectories have spatial uncertainties, especially with increasing length of time and distance from the starting location. Yet, this methodology showed trends in cloud water composition consistent with smoke influence, as shown in previous air quality studies using the same methodology (Brey, Ruminski, et al., 2018; O'Dell et al., 2019). Future work is needed to develop widely accessible methodologies to identify smoke plumes spatially, vertically, and by age for long-term monitoring studies.

Cloud water composition varied between smoke classifications. Significant differences between smoke classifications were observed for ozone, carbon monoxide, inorganic ion concentrations, and TOC. Elevated ozone and carbon monoxide levels have been associated with the presence of long-range transported smoke (Jaffe & Wigder, 2012; Selimovic et al., 2020), impacting regional air quality and climate far from the fire source (Briggs et al., 2017; Dreessen et al., 2016; Rogers et al., 2020). Specifically, cloud water samples with high probability of smoke influence showed significantly higher concentrations compared to samples with a low probability of smoke influence for K^+, SO_4^{2-}, NH_4^+, and TOC, all of which have been previously identified in cloud water influenced by biomass burning events (Budhavant et al., 2014; Stahl et al., 2021). Previous wildfire influenced cloud water studies have suggested that the TOC composition may contain carbonyls, carboxylic acids, nitrogen-containing compounds, oligomeric species, and light absorbing secondary organic aerosols formed within clouds (Cook et al., 2017; Li et al., 2020; Schurman et al., 2018; Sun et al., 2021; Tomaz et al., 2018). These results suggest long-range transported smoke frequently alters the chemical composition of cloud water

at Whiteface Mountain. Further work is needed to investigate the molecular composition of wildfire-influenced cloud water and to distinguish primary organic compounds emitted directly from secondary products, including those formed within cloud droplets.

Case samples were selected to further examine the properties and composition of smoke-influenced cloud water samples. All five case study samples (three classified as having a high probability of smoke influence and two classified as having a low smoke probability) contained low concentrations of levoglucosan (0.2–0.9 μM), a common tracer for biomass burning, with degradation of levoglucosan during transport likely influencing the levels. The case study samples highlighted the influence of backward air mass trajectories on cloud water composition. Regardless of smoke classification, samples featuring air masses transiting within the atmospheric boundary layer, particularly over urban areas, had higher sulfate and nitrate concentrations and higher insoluble particle concentrations, with smaller mode diameters, compared to cloud water samples with air masses that remained aloft during transport. In comparison, the samples that had their air masses remain aloft during transport contained greater concentrations of cloud processed organic acids such as oxalate. Two case samples, with differing probabilities of smoke influence, had sufficient volume to measure UV-visible absorbing compounds. Previous studies have suggested that concentrations of UV-visible absorbing compounds in cloud water, whether partitioned into or produced in the aqueous-phase, increases as biomass burning aerosols age (Desyaterik et al., 2013; Di Lorenzo et al., 2017; Hawkins et al., 2018; Hecobian et al., 2010; Hems et al., 2020, 2021; Zhang et al., 2011). The absorbing compounds could include humic-like substances (HULIS), aromatic compounds, high molecular weight molecules, and nitrophenol derivatives that are present in brown carbon (Desyaterik et al., 2013; Di Lorenzo et al., 2017; Hawkins et al., 2018; Hecobian et al., 2010; Hems et al., 2020, 2021; Zhang et al., 2011). The two samples were additionally influenced by urban emissions and had measurable MAC_{365} and AAE values, showing the presence of radiation absorbing compounds. These results motivate further studies to investigate how smoke and urban air masses mix to jointly impact cloud composition. Further work is also needed to investigate cloud water composition influenced by smoke and the impacts on cloud radiative and microphysical properties as smoke particles undergo cloud processing, particularly in the context of increasing wildfires (Flannigan et al., 2013; Jolly et al., 2015; Westerling, 2016).

Data Availability Statement

The cloud water and trace gas monitoring data sets used herein are available through the Adirondack Lake Survey Corporation (ALSC (2022), http://www.adirondacklakessurvey.org/wfc.shtml) and the University of Albany Atmospheric Sciences Research Center's Air Quality Monitoring Products (ASRC (2022), http://atmoschem.asrc.cestm.albany.edu/). The backward air mass trajectories were obtained through the NOAA Hybrid Single Particle Lagrangian Integrated Trajectory (HYSPLIT) Model (Rolph et al., 2017; Stein et al., 2015) available online (https://www.ready.noaa.gov/HYSPLIT_traj.php). Smoke was identified using the NOAA Hazard Mapping System Fire and Smoke Product (Rolph et al., 2009) downloaded online (https://www.ospo.noaa.gov/Products/land/hms.html).

Acknowledgments
We thank James E. Dukett (formerly of the Adirondack Lake Survey Corp.) for provision of the cloud water samples and discussions. We thank the University of Albany Atmospheric Sciences Research Center and Scott McKim for the trace gas observations from the summit of Whiteface Mountain. The authors thank Jun Liu, Alexa Watson, Jia Shi, and Andrew Ault (University of Michigan) for discussions. L. Vear was funded through the University of Michigan Authentic Research Connection program funded by the Howard Hughes Medical Institute (52008119). N. Olson was funded through the Michigan Sea Grant College Program (project number 1026019353) under NA18OAR4170102 from National Sea Grant, National Oceanic and Atmospheric Administration (NOAA), U.S. Department of Commerce, with funds from the State of Michigan. Additional funding for N. Olson, L. Vear, R. Cook, and J. Lee was provided by the University of Michigan Department of Chemistry. This work was inspired by the Mountain Top Cloud Sampling: Experimental Design for Coordinated Study of Multiphase Chemical Mechanism Workshop, funded by the National Science Foundation (AGS-1638579). The authors acknowledge the NOAA Air Resources Laboratory (ARL) for the provision of the HYSPLIT transport and dispersion model and READY website (https://www.ready.noaa.gov) used in this publication. The authors thank the analysts who developed and maintain the NESDIS Hazard Mapping System Fire and Smoke Product. We thank the Harvey Mudd College Chemistry 40 Spring 2019 students for their help in analyzing the UV/visible absorbance of the cloud water samples.

References

Ahern, A. T., Robinson, E. S., Tkacik, D. S., Saleh, R., Hatch, L. E., Barsanti, K. C., et al. (2019). Production of secondary organic aerosol during aging of biomass burning smoke from fresh fuels and its relationship to VOC precursors. *Journal of Geophysical Research: Atmospheres*, *124*(6), 3583–3606. https://doi.org/10.1029/2018JD029068

Akagi, S. K., Yokelson, R. J., Burling, I. R., Meinardi, S., Simpson, I., Blake, D. R., et al. (2013). Measurements of reactive trace gases and variable O_3 formation rates in some South Carolina biomass burning plumes. *Atmospheric Chemistry and Physics*, *13*(3), 1141–1165. https://doi.org/10.5194/acp-13-1141-2013

Aleksic, N., & Dukett, J. E. (2010). Probabilistic relationship between liquid water content and ion concentrations in cloud water. *Atmospheric Research*, *98*(2), 400–405. https://doi.org/10.1016/j.atmosres.2010.08.003

Aleksic, N., Roy, K., Sistla, G., Dukett, J., Houck, N., & Casson, P. (2009). Analysis of cloud and precipitation chemistry at Whiteface Mountain, NY. *Atmospheric Environment*, *43*(17), 2709–2716. https://doi.org/10.1016/j.atmosenv.2009.02.053

ALSC. (2022). Whiteface mountain cloud monitoring chemistry and sample associated meteorological data [Dataset]. Retrieved from http://www.adirondacklakessurvey.org/wfc.shtml

Andreae, M. O., Rosenfeld, D., Artaxo, P., Costa, A. A., Frank, G. P., Longo, K. M., & Silva-Dias, M. A. F. (2004). Smoking rain clouds over the Amazon. *Science*, *303*(5662), 1337–1342. https://doi.org/10.1126/science.1092779

Aquila, V., Hendricks, J., Lauer, A., Riemer, N., Vogel, H., Baumgardner, D., et al. (2011). MADE-in: A new aerosol microphysics submodel for global simulation of insoluble particles and their mixing state. *Geoscientific Model Development*, *4*(2), 325–355. https://doi.org/10.5194/gmd-4-325-2011

ASRC. (2022). ASRC AQM data products [Dataset]. Retrieved from http://atmoschem.asrc.cestm.albany.edu/

Axson, J. L., Creamean, J. M., Bondy, A. L., Capracotta, S. S., Warner, K. Y., & Ault, A. P. (2015). An in situ method for sizing insoluble residues in precipitation and other aqueous samples. *Aerosol Science and Technology*, *49*(1), 24–34. https://doi.org/10.1080/02786826.2014.991439

Axson, J. L., Shen, H., Bondy, A. L., Landry, C. C., Welz, J., Creamean, J. M., & Ault, A. P. (2016). Transported mineral dust deposition case study at a hydrologically sensitive mountain site: Size and composition shifts in ambient aerosol and snowpack. *Aerosol and Air Quality Research*, *16*(3), 555–567. https://doi.org/10.4209/aaqr.2015.05.0346

Bai, J., Sun, X., Zhang, C., Xu, Y., & Qi, C. (2013). The OH-initiated atmospheric reaction mechanism and kinetics for levoglucosan emitted in biomass burning. *Chemosphere*, *93*(9), 2004–2010. https://doi.org/10.1016/j.chemosphere.2013.07.021

Baumgardner, R. E., Isil, S. S., Lavery, T. F., Rogers, C. M., & Mohnen, V. A. (2003). Estimates of cloud water deposition at mountain acid deposition program sites in the Appalachian mountains. *Journal of the Air & Waste Management Association*, *53*(3), 291–308. https://doi.org/10.1080/10473289.2003.10466153

Baumgardner, R. E., Kronmiller, K. G., Anderson, J. B., Bowser, J. J., & Edgerton, E. S. (1997). Development of an automated cloud water collection system for use in atmospheric monitoring networks. *Atmospheric Environment*, *31*(13), 2003–2010. https://doi.org/10.1016/s1352-2310(96)00325-1

Becidan, M., Skreiberg, Ø., & Hustad, J. E. (2007). NOx and N_2O precursors (NH_3 and HCN) in pyrolysis of biomass residues. *Energy & Fuels*, *21*(2), 1173–1180. https://doi.org/10.1021/ef060426k

Bian, Q., Ford, B., Pierce, J. R., & Kreidenweis, S. M. (2020). A decadal climatology of chemical, physical, and optical properties of ambient smoke in the western and southeastern United States. *Journal of Geophysical Research: Atmospheres*, *125*(1), e2019JD031372. https://doi.org/10.1029/2019JD031372

Blanchard, C. L., Shaw, S. L., Edgerton, E. S., & Schwab, J. J. (2019). Emission influences on air pollutant concentrations in New York state: II. PM2.5 organic and elemental carbon constituents. *Atmospheric Environment X*, *3*, 100039. https://doi.org/10.1016/j.aeaoa.2019.100039

Blando, J. D., & Turpin, B. J. (2000). Secondary organic aerosol formation in cloud and fog droplets: A literature evaluation of plausibility. *Atmospheric Environment*, *34*(10), 1623–1632. https://doi.org/10.1016/s1352-2310(99)00392-1

Bougiatioti, A., Bezantakos, S., Stavroulas, I., Kalivitis, N., Kokkalis, P., Biskos, G., et al. (2016). Biomass-burning impact on CCN number, hygroscopicity and cloud formation during summertime in the eastern Mediterranean. *Atmospheric Chemistry and Physics*, *16*(11), 7389–7409. https://doi.org/10.5194/acp-16-7389-2016

Brandt, R. E., Schwab, J. J., Casson, P. W., Roychowdhury, U. K., Wolfe, D., Demerjian, K. L., et al. (2016). Atmospheric chemistry measurements at whiteface mountain, NY: Ozone and reactive trace gases. *Aerosol and Air Quality Research*, *16*(3), 873–884. https://doi.org/10.4209/aaqr.2015.05.0376

Brey, S. J., Barnes, E. A., Pierce, J. R., Wiedinmyer, C., & Fischer, E. V. (2018). Environmental conditions, ignition type, and air quality impacts of wildfires in the southeastern and Western United States. *Earth's Future*, *6*(10), 1442–1456. https://doi.org/10.1029/2018EF000972

Brey, S. J., Ruminski, M., Atwood, S. A., & Fischer, E. V. (2018). Connecting smoke plumes to sources using Hazard Mapping System (HMS) smoke and fire location data over North America. *Atmospheric Chemistry and Physics*, *18*(3), 1745–1761. https://doi.org/10.5194/acp-18-1745-2018

Briggs, N. L., Jaffe, D. A., Gao, H., Hee, J. R., Baylon, P. M., Zhang, Q., et al. (2017). Particulate matter, ozone, and nitrogen species in aged wildfire plumes observed at the Mount bachelor observatory. *Aerosol and Air Quality Research*, *16*(12), 3075–3087. https://doi.org/10.4209/aaqr.2016.03.0120

Budhavant, K. B., Rao, P. S. P., Safai, P. D., Granat, L., & Rodhe, H. (2014). Chemical composition of the inorganic fraction of cloud-water at a high altitude station in West India. *Atmospheric Environment*, *88*, 59–65. https://doi.org/10.1016/j.atmosenv.2014.01.039

Chan, M. N., Kreidenweis, S. M., & Chan, C. K. (2008). Measurements of the hygroscopic and deliquescence properties of organic compounds of different solubilities in water and their relationship with cloud condensation nuclei activities. *Environmental Science & Technology*, *42*(10), 3602–3608. https://doi.org/10.1021/es7023252

Chen, J., Li, C., Ristovski, Z., Milic, A., Gu, Y., Islam, M. S., et al. (2017). A review of biomass burning: Emissions and impacts on air quality, health and climate in China. *Science of The Total Environment*, *579*, 1000–1034. https://doi.org/10.1016/j.scitotenv.2016.11.025

Chen, Q., Heald, C. L., Jimenez, J. L., Canagaratna, M. R., Zhang, Q., He, L.-Y., et al. (2015). Elemental composition of organic aerosol: The gap between ambient and laboratory measurements. *Geophysical Research Letters*, *42*(10), 4182–4189. https://doi.org/10.1002/2015GL063693

Cheng, Y., He, K. B., Zheng, M., Duan, F. K., Du, Z. Y., Ma, Y. L., et al. (2011). Mass absorption efficiency of elemental carbon and water-soluble organic carbon in Beijing, China. *Atmospheric Chemistry and Physics*, *11*(22), 11497–11510. https://doi.org/10.5194/acp-11-11497-2011

Chuang, M.-T., Fu, J. S., Lee, C.-T., Lin, N.-H., Gao, Y., Wang, S.-H., et al. (2016). The simulation of long-range transport of biomass burning plume and short-range transport of anthropogenic pollutants to a mountain observatory in East Asia during the 7-SEAS/2010 Dongsha experiment. *Aerosol and Air Quality Research*, *16*(11), 2933–2949. https://doi.org/10.4209/aaqr.2015.07.0440

Cook, R. D., Lin, Y. H., Peng, Z., Boone, E., Chu, R. K., Dukett, J. E., et al. (2017). Biogenic, urban, and wildfire influences on the molecular composition of dissolved organic compounds in cloud water. *Atmospheric Chemistry and Physics*, *17*(24), 15167–15180. https://doi.org/10.5194/acp-17-15167-2017

DeBell, L. J., Talbot, R. W., Dibb, J. E., Munger, J. W., Fischer, E. V., & Frolking, S. E. (2004). A major regional air pollution event in the northeastern United States caused by extensive forest fires in Quebec, Canada. *Journal of Geophysical Research*, *109*(D19), D19305. https://doi.org/10.1029/2004JD004840

De Haan, D. O., Jansen, K., Rynaski, A. D., Sueme, W. R. P., Torkelson, A. K., Czer, E. T., et al. (2020). Brown carbon production by aqueous-phase interactions of glyoxal and SO_2. *Environmental Science & Technology*, *54*(8), 4781–4789. https://doi.org/10.1021/acs.est.9b07852

Dennison, P. E., Brewer, S. C., Arnold, J. D., & Moritz, M. A. (2014). Large wildfire trends in the western United States, 1984–2011. *Geophysical Research Letters*, *41*(8), 2928–2933. https://doi.org/10.1002/2014GL059576

Desyaterik, Y., Sun, Y., Shen, X., Lee, T., Wang, X., Wang, T., & Collett, J. L., Jr. (2013). Speciation of "brown" carbon in cloud water impacted by agricultural biomass burning in eastern China. *Journal of Geophysical Research: Atmospheres*, *118*(13), 7389–7399. https://doi.org/10.1002/jgrd.50561

Di Lorenzo, R. A., Washenfelder, R. A., Attwood, A. R., Guo, H., Xu, L., Ng, N. L., et al. (2017). Molecular-size-separated brown carbon absorption for biomass-burning aerosol at multiple field sites. *Environmental Science & Technology*, *51*(6), 3128–3137. https://doi.org/10.1021/acs.est.6b06160

Dreessen, J., Sullivan, J., & Delgado, R. (2016). Observations and impacts of transported Canadian wildfire smoke on ozone and aerosol air quality in the Maryland region on June 9–12, 2015. *Journal of the Air & Waste Management Association*, *66*(9), 842–862. https://doi.org/10.1080/10962247.2016.1161674

Engelhart, G. J., Hennigan, C. J., Miracolo, M. A., Robinson, A. L., & Pandis, S. N. (2012). Cloud condensation nuclei activity of fresh primary and aged biomass burning aerosol. *Atmospheric Chemistry and Physics*, *12*(15), 7285–7293. https://doi.org/10.5194/acp-12-7285-2012

Engling, G., Lee, J. J., Tsai, Y.-W., Lung, S.-C. C., Chou, C. C. K., & Chan, C.-Y. (2009). Size-resolved anhydrosugar composition in smoke aerosol from controlled field burning of rice straw. *Aerosol Science and Technology*, *43*(7), 662–672. https://doi.org/10.1080/02786820902825113

Ervens, B., Cubison, M. J., Andrews, E., Feingold, G., Ogren, J. A., Jimenez, J. L., et al. (2010). CCN predictions using simplified assumptions of organic aerosol composition and mixing state: A synthesis from six different locations. *Atmospheric Chemistry and Physics*, *10*(10), 4795–4807. https://doi.org/10.5194/acp-10-4795-2010

Ervens, B., Feingold, G., Frost, G. J., & Kreidenweis, S. M. (2004). A modeling study of aqueous production of dicarboxylic acids: 1. Chemical pathways and speciated organic mass production. *Journal of Geophysical Research*, *109*(D15), D15205. Retrieved from https://agupubs.onlinelibrary.wiley.com/doi/abs/10.1029/2003JD004387

Ervens, B., Turpin, B. J., & Weber, R. J. (2011). Secondary organic aerosol formation in cloud droplets and aqueous particles (aqSOA): A review of laboratory, field and model studies. *Atmospheric Chemistry and Physics*, *11*(21), 11069–11102. https://doi.org/10.5194/acp-11-11069-2011

Fabbri, D., Torri, C., Simoneit, B. R. T., Marynowski, L., Rushdi, A. I., & Fabiańska, M. J. (2009). Levoglucosan and other cellulose and lignin markers in emissions from burning of Miocene lignites. *Atmospheric Environment*, *43*(14), 2286–2295. https://doi.org/10.1016/j.atmosenv.2009.01.030

Falconer, R. E., & Falconer, P. D. (1980). Determination of cloud water acidity at a mountain observatory in the Adirondack Mountains of New York State. *Journal of Geophysical Research*, *85*(C12), 7465–7470. https://doi.org/10.1029/JC085iC12p07465

Flannigan, M., Cantin, A. S., de Groot, W. J., Wotton, M., Newbery, A., & Gowman, L. M. (2013). Global wildland fire season severity in the 21st century. *Forest Ecology and Management*, *294*, 54–61. https://doi.org/10.1016/j.foreco.2012.10.022

Furutani, H., Dall'osto, M., Roberts, G. C., & Prather, K. A. (2008). Assessment of the relative importance of atmospheric aging on CCN activity derived from field observations. *Atmospheric Environment*, *42*(13), 3130–3142. https://doi.org/10.1016/j.atmosenv.2007.09.024

Gao, S., Hegg, D. A., Hobbs, P. V., Kirchstetter, T. W., Magi, B. I., & Sadilek, M. (2003). Water-soluble organic components in aerosols associated with savanna fires in southern Africa: Identification, evolution, and distribution. *Journal of Geophysical Research*, *108*(D13). https://doi.org/10.1029/2002JD002324

Ge, C., Wang, J., & Reid, J. S. (2014). Mesoscale modeling of smoke transport over the southeast Asian Maritime continent: Coupling of smoke direct radiative effect below and above the low-level clouds. *Atmospheric Chemistry and Physics*, *14*(1), 159–174. https://doi.org/10.5194/acp-14-159-2014

Gerber, H. (1991). Direct measurement of suspended particulate volume concentration and far-infrared extinction coefficient with a laser-diffraction instrument. *Applied Optics*, *30*(33), 4824–4831. Retrieved from http://opg.optica.org/ao/abstract.cfm?URI=ao-30-33-4824

Ghan, S. J., Liu, X., Easter, R. C., Zaveri, R., Rasch, P. J., Yoon, J. H., & Eaton, B. (2012). Toward a minimal representation of aerosols in climate models: Comparative decomposition of aerosol direct, semidirect, and indirect radiative forcing. *Journal of Climate*, *25*(19), 6461–6476. https://doi.org/10.1175/jcli-d-11-00650.1

Giebl, H., Berner, A., Reischl, G., Puxbaum, H., Kasper-Giebl, A., & Hitzenberger, R. (2002). CCN activation of oxalic and malonic acid test aerosols with the University of Vienna cloud condensation nuclei counter. *Journal of Aerosol Science*, *33*(12), 1623–1634. https://doi.org/10.1016/s0021-8502(02)00115-5

Gilardoni, S., Massoli, P., Marinoni, A., Mazzoleni, C., Freedman, A., Lonati, G., et al. (2020). Spatial and temporal variability of carbonaceous aerosol absorption in the Po valley. *Aerosol and Air Quality Research*, *20*(12), 2624–2639. https://doi.org/10.4209/aaqr.2020.03.0085

Gilardoni, S., Massoli, P., Paglione, M., Giulianelli, L., Carbone, C., Rinaldi, M., et al. (2016). Direct observation of aqueous secondary organic aerosol from biomass-burning emissions. *Proceedings of the National Academy of Sciences*, *113*(36), 10013–10018. https://doi.org/10.1073/pnas.1602212113

Gilman, J. B., Lerner, B. M., Kuster, W. C., Goldan, P. D., Warneke, C., Veres, P. R., et al. (2015). Biomass burning emissions and potential air quality impacts of volatile organic compounds and other trace gases from fuels common in the US. *Atmospheric Chemistry and Physics*, *15*(24), 13915–13938. https://doi.org/10.5194/acp-15-13915-2015

Gioda, A., Mayol-Bracero, O. L., Reyes-Rodriguez, G. J., Santos-Figueroa, G., & Collett, J. L. (2008). Water-soluble organic and nitrogen levels in cloud and rainwater in a background marine environment under influence of different air masses. *Journal of Atmospheric Chemistry*, *61*(2), 85–99. https://doi.org/10.1007/s10874-009-9125-6

Grandey, B. S., Lee, H. H., & Wang, C. (2016). Radiative effects of interannually varying vs. interannually invariant aerosol emissions from fires. *Atmospheric Chemistry and Physics*, *16*(22), 14495–14513. https://doi.org/10.5194/acp-16-14495-2016

Hawkins, L. N., Welsh, H. G., & Alexander, M. V. (2018). Evidence for pyrazine-based chromophores in cloud water mimics containing methylglyoxal and ammonium sulfate. *Atmospheric Chemistry and Physics*, *18*(16), 12413–12431. https://doi.org/10.5194/acp-18-12413-2018

Haywood, J., & Boucher, O. (2000). Estimates of the direct and indirect radiative forcing due to tropospheric aerosols: A review. *Reviews of Geophysics*, *38*(4), 513–543. https://doi.org/10.1029/1999RG000078

Hecobian, A., Liu, Z., Hennigan, C. J., Huey, L. G., Jimenez, J. L., Cubison, M. J., et al. (2011). Comparison of chemical characteristics of 495 biomass burning plumes intercepted by the NASA DC-8 aircraft during the ARCTAS/CARB-2008 field campaign. *Atmospheric Chemistry and Physics*, *11*(24), 13325–13337. https://doi.org/10.5194/acp-11-13325-2011

Hecobian, A., Zhang, X., Zheng, M., Frank, N., Edgerton, E. S., & Weber, R. J. (2010). Water-soluble organic aerosol material and the light-absorption characteristics of aqueous extracts measured over the Southeastern United States. *Atmospheric Chemistry and Physics*, *10*(13), 5965–5977. https://doi.org/10.5194/acp-10-5965-2010

Hems, R. F., Schnitzler, E. G., Bastawrous, M., Soong, R., Simpson, A. J., & Abbatt, J. P. D. (2020). Aqueous photoreactions of wood smoke brown carbon. *ACS Earth and Space Chemistry*, *4*(7), 1149–1160. https://doi.org/10.1021/acsearthspacechem.0c00117

Hems, R. F., Schnitzler, E. G., Liu-Kang, C., Cappa, C. D., & Abbatt, J. P. D. (2021). Aging of atmospheric brown carbon aerosol. *ACS Earth and Space Chemistry*, *5*(4), 722–748. https://doi.org/10.1021/acsearthspacechem.0c00346

Hennigan, C. J., Sullivan, A. P., Collett, J. L., Jr., & Robinson, A. L. (2010). Levoglucosan stability in biomass burning particles exposed to hydroxyl radicals. *Geophysical Research Letters*, *37*(9), GL043088. https://doi.org/10.1029/2010GL043088

Herckes, P., Valsaraj, K. T., & Collett, J. L. (2013). A review of observations of organic matter in fogs and clouds: Origin, processing and fate. *Atmospheric Research*, *132–133*, 434–449. https://doi.org/10.1016/j.atmosres.2013.06.005

Hilario, M. R. A., Crosbie, E., Bañaga, P. A., Betito, G., Braun, R. A., Cambaliza, M. O., et al. (2021). Particulate oxalate-to-sulfate ratio as an aqueous processing marker: Similarity across field campaigns and limitations. *Geophysical Research Letters*, *48*(23), e2021GL096520. https://doi.org/10.1029/2021GL096520

Hodshire, A. L., Akherati, A., Alvarado, M. J., Brown-Steiner, B., Jathar, S. H., Jimenez, J. L., et al. (2019). Aging effects on biomass burning aerosol mass and composition: A critical review of field and laboratory studies. *Environmental Science & Technology*, *53*(17), 10007–10022. https://doi.org/10.1021/acs.est.9b02588

Hoffmann, D., Tilgner, A., Iinuma, Y., & Herrmann, H. (2010). Atmospheric stability of levoglucosan: A detailed laboratory and modeling study. *Environmental Science & Technology*, *44*(2), 694–699. https://doi.org/10.1021/es902476f

Hudson, J. G. (1991). Observations of anthropogenic cloud condensation nuclei. *Atmospheric Environment, Part A: General Topics*, *25*(11), 2449–2455. https://doi.org/10.1016/0960-1686(91)90162-z

Hudson, P. K., Murphy, D. M., Cziczo, D. J., Thomson, D. S., de Gouw, J. A., Warneke, C., et al. (2004). Biomass-burning particle measurements: Characteristic composition and chemical processing. *Journal of Geophysical Research*, *109*(D23), D004398. https://doi.org/10.1029/2003JD004398

Hung, W.-T., Lu, C.-H., Alessandrini, S., Kumar, R., & Lin, C.-A. (2021). The impacts of transported wildfire smoke aerosols on surface air quality in New York state: A multi-year study using machine learning. *Atmospheric Environment*, *259*, 118513. https://doi.org/10.1016/j.atmosenv.2021.118513

Hutchings, J. W., Robinson, M. S., McIlwraith, H., Triplett Kingston, J., & Herckes, P. (2009). The chemistry of intercepted clouds in Northern Arizona during the North American Monsoon season. *Water, Air, and Soil Pollution*, *199*(1), 191–202. https://doi.org/10.1007/s11270-008-9871-0

Jacob, D. J., Crawford, J. H., Maring, H., Clarke, A. D., Dibb, J. E., Emmons, L. K., et al. (2010). The Arctic Research of the composition of the troposphere from aircraft and satellites (ARCTAS) mission: Design, execution, and first results. *Atmospheric Chemistry and Physics*, *10*(11), 5191–5212. https://doi.org/10.5194/acp-10-5191-2010

Jaffe, D. A., O'Neill, S. M., Larkin, N. K., Holder, A. L., Peterson, D. L., Halofsky, J. E., & Rappold, A. G. (2020). Wildfire and prescribed burning impacts on air quality in the United States. *Journal of the Air & Waste Management Association*, *70*(6), 583–615. https://doi.org/10.1080/10962247.2020.1749731

Jaffe, D. A., & Wigder, N. L. (2012). Ozone production from wildfires: A critical review. *Atmospheric Environment*, *51*, 1–10. https://doi.org/10.1016/j.atmosenv.2011.11.063

Jing, B., Wang, Z., Tan, F., Guo, Y., Tong, S., Wang, W., et al. (2018). Hygroscopic behavior of atmospheric aerosols containing nitrate salts and water-soluble organic acids. *Atmospheric Chemistry and Physics*, *18*(7), 5115–5127. https://doi.org/10.5194/acp-18-5115-2018

Jolly, W. M., Cochrane, M. A., Freeborn, P. H., Holden, Z. A., Brown, T. J., Williamson, G. J., & Bowman, D. M. J. S. (2015). Climate-induced variations in global wildfire danger from 1979 to 2013. *Nature Communications*, *6*(1), 7537. Article. https://doi.org/10.1038/ncomms8537

Kawamura, K., & Gagosian, R. B. (1987). Implications of ω-oxocarboxylic acids in the remote marine atmosphere for photo-oxidation of unsaturated fatty acids. *Nature*, *325*(6102), 330–332. https://doi.org/10.1038/325330a0

Khalizov, A. F., Zhang, R., Zhang, D., Xue, H., Pagels, J., & McMurry, P. H. (2009). Formation of highly hygroscopic soot aerosols upon internal mixing with sulfuric acid vapor. *Journal of Geophysical Research*, *114*(D5), D05208. https://doi.org/10.1029/2008JD010595

Khwaja, H. A., Brudnoy, S., & Husain, L. (1995). Chemical characterization of three summer cloud episodes at whiteface mountain. *Chemosphere*, *31*(5), 3357–3381. https://doi.org/10.1016/0045-6535(95)00187-d

Kirillova, E. N., Andersson, A., Han, J., Lee, M., & Gustafsson, Ö. (2014). Sources and light absorption of water-soluble organic carbon aerosols in the outflow from northern China. *Atmospheric Chemistry and Physics*, *14*(3), 1413–1422. https://doi.org/10.5194/acp-14-1413-2014

Kleinman, L. I., Sedlacek, A. J., Iii, Adachi, K., Buseck, P. R., Collier, S., Dubey, M. K., et al. (2020). Rapid evolution of aerosol particles and their optical properties downwind of wildfires in the western US. *Atmospheric Chemistry and Physics*, *20*(21), 13319–13341. https://doi.org/10.5194/acp-20-13319-2020

Lai, C., Liu, Y., Ma, J., Ma, Q., & He, H. (2014). Degradation kinetics of levoglucosan initiated by hydroxyl radical under different environmental conditions. *Atmospheric Environment*, *91*, 32–39. https://doi.org/10.1016/j.atmosenv.2014.03.054

Lance, S., Barth, M., & Carlton, A. (2017). Multiphase chemistry: Experimental design for coordinated measurement and modeling studies of cloud processing at a mountaintop. *Bulletin of the American Meteorological Society*, *98*(7), ES163–ES167. https://doi.org/10.1175/bams-d-17-0015.1

Lance, S., Zhang, J., Schwab, J. J., Casson, P., Brandt, R. E., Fitzjarrald, D. R., et al. (2020). Overview of the CPOC pilot study at whiteface mountain, NY: Cloud processing of organics within clouds (CPOC). *Bulletin of the American Meteorological Society*, *101*(10), E1820–E1841. https://doi.org/10.1175/bams-d-19-0022.1

Larsen, A. E., Reich, B. J., Ruminski, M., & Rappold, A. G. (2018). Impacts of fire smoke plumes on regional air quality, 2006–2013. *Journal of Exposure Science and Environmental Epidemiology*, *28*(4), 319–327. https://doi.org/10.1038/s41370-017-0013-x

Lee, A. K. Y., Hayden, K. L., Herckes, P., Leaitch, W. R., Liggio, J., Macdonald, A. M., & Abbatt, J. P. D. (2012). Characterization of aerosol and cloud water at a mountain site during WACS 2010: Secondary organic aerosol formation through oxidative cloud processing. *Atmospheric Chemistry and Physics*, *12*(15), 7103–7116. https://doi.org/10.5194/acp-12-7103-2012

Lee, H. H., & Wang, C. (2020). The impacts of biomass burning activities on convective systems over the Maritime Continent. *Atmospheric Chemistry and Physics*, *20*(4), 2533–2548. https://doi.org/10.5194/acp-20-2533-2020

Leskinen, A. P., Jokiniemi, J. K., & Lehtinen, K. E. J. (2007). Characterization of aging wood chip combustion aerosol in an environmental chamber. *Atmospheric Environment*, *41*(17), 3713–3721. https://doi.org/10.1016/j.atmosenv.2006.12.016

Li, T., Wang, Z., Wang, Y., Wu, C., Liang, Y., Xia, M., et al. (2020). Chemical characteristics of cloud water and the impacts on aerosol properties at a subtropical mountain site in Hong Kong SAR. *Atmospheric Chemistry and Physics*, *20*(1), 391–407. https://doi.org/10.5194/acp-20-391-2020

Li, Y. (2019). Cloud condensation nuclei activity and hygroscopicity of fresh and aged biomass burning particles. *Pure and Applied Geophysics*, *176*(1), 345–356. https://doi.org/10.1007/s00024-018-1903-0

Lim, C. Y., Hagan, D. H., Coggon, M. M., Koss, A. R., Sekimoto, K., de Gouw, J., et al. (2019). Secondary organic aerosol formation from the laboratory oxidation of biomass burning emissions. *Atmospheric Chemistry and Physics*, *19*(19), 12797–12809. https://doi.org/10.5194/acp-19-12797-2019

Liu, J. C., Mickley, L. J., Sulprizio, M. P., Dominici, F., Yue, X., Ebisu, K., et al. (2016). Particulate air pollution from wildfires in the Western US under climate change. *Climatic Change*, *138*(3), 655–666. https://doi.org/10.1007/s10584-016-1762-6

Liu, X., Huey, L. G., Yokelson, R. J., Selimovic, V., Simpson, I. J., Müller, M., et al. (2017). Airborne measurements of western U.S. wildfire emissions: Comparison with prescribed burning and air quality implications. *Journal of Geophysical Research: Atmospheres*, *122*(11), 6108–6129. https://doi.org/10.1002/2016JD026315

Liu, Y., Stanturf, J., & Goodrick, S. (2010). Trends in global wildfire potential in a changing climate. *Forest Ecology and Management*, *259*(4), 685–697. https://doi.org/10.1016/j.foreco.2009.09.002

Lohmann, U., & Feichter, J. (2005). Global indirect aerosol effects: A review. *Atmospheric Chemistry and Physics*, *5*(3), 715–737. https://doi.org/10.5194/acp-5-715-2005

Lu, Z., & Sokolik, I. N. (2013). The effect of smoke emission amount on changes in cloud properties and precipitation: A case study of Canadian boreal wildfires of 2007. *Journal of Geophysical Research: Atmospheres*, *118*(20), 11777–11793. https://doi.org/10.1002/2013JD019860

MacDougall, D., & Crummett, W. B. (1980). Guidelines for data acquisition and data quality evaluation in environmental chemistry. *Analytical Chemistry*, *52*(14), 2242–2249. https://doi.org/10.1021/ac50064a004

Matz, C. J., Egyed, M., Xi, G., Racine, J., Pavlovic, R., Rittmaster, R., et al. (2020). Health impact analysis of PM2.5 from wildfire smoke in Canada (2013–2015, 2017–2018). *Science of The Total Environment*, *725*, 138506. https://doi.org/10.1016/j.scitotenv.2020.138506

May, A. A., McMeeking, G. R., Lee, T., Taylor, J. W., Craven, J. S., Burling, I., et al. (2014). Aerosol emissions from prescribed fires in the United States: A synthesis of laboratory and aircraft measurements. *Journal of Geophysical Research: Atmospheres*, *119*(20), 11826–11849. https://doi.org/10.1002/2014JD021848

May, N. W., Gunsch, M. J., Olson, N. E., Bondy, A. L., Kirpes, R. M., Bertman, S. B., et al. (2018). Unexpected contributions of sea spray and lake spray aerosol to inland particulate matter. *Environmental Science and Technology Letters*, *5*(7), 405–412. https://doi.org/10.1021/acs.estlett.8b00254

McClure, C. D., & Jaffe, D. A. (2018). US particulate matter air quality improves except in wildfire-prone areas. *Proceedings of the National Academy of Sciences*, *115*(31), 7901–7906. https://doi.org/10.1073/pnas.1804353115

McCluskey, C. S., DeMott, P. J., Prenni, A. J., Levin, E. J. T., McMeeking, G. R., Sullivan, A. P., et al. (2014). Characteristics of atmospheric ice nucleating particles associated with biomass burning in the US: Prescribed burns and wildfires. *Journal of Geophysical Research: Atmospheres*, *119*(17), 10458–10470. https://doi.org/10.1002/2014JD021980

McFiggans, G., Artaxo, P., Baltensperger, U., Coe, H., Facchini, M. C., Feingold, G., et al. (2006). The effect of physical and chemical aerosol properties on warm cloud droplet activation. *Atmospheric Chemistry and Physics*, *6*(9), 2593–2649. https://doi.org/10.5194/acp-6-2593-2006

Mekis, E., Donaldson, N., Reid, J., Zucconi, A., Hoover, J., Li, Q., et al. (2018). An overview of surface-based precipitation observations at environment and climate change Canada. *Atmosphere-Ocean*, *56*(2), 71–95. https://doi.org/10.1080/07055900.2018.1433627

Nikonovas, T., North, P. R. J., & Doerr, S. H. (2015). Smoke aerosol properties and ageing effects for northern temperate and boreal regions derived from AERONET source and age attribution. *Atmospheric Chemistry and Physics*, *15*(14), 7929–7943. https://doi.org/10.5194/acp-15-7929-2015

O'Dell, K., Bilsback, K., Ford, B., Martenies, S. E., Magzamen, S., Fischer, E. V., & Pierce, J. R. (2021). Estimated mortality and morbidity attributable to smoke plumes in the United States: Not just a western US problem. *GeoHealth*, *5*(9), e2021GH000457. https://doi.org/10.1029/2021GH000457

O'Dell, K., Ford, B., Fischer, E. V., & Pierce, J. R. (2019). Contribution of wildland-fire smoke to US $PM_{2.5}$ and its influence on recent trends. *Environmental Science & Technology*, *53*(4), 1797–1804. https://doi.org/10.1021/acs.est.8b05430

Park, R. J., Jacob, D. J., & Logan, J. A. (2007). Fire and biofuel contributions to annual mean aerosol mass concentrations in the United States. *Atmospheric Environment*, *41*(35), 7389–7400. https://doi.org/10.1016/j.atmosenv.2007.05.061

Paulot, F., Wunch, D., Crounse, J. D., Toon, G. C., Millet, D. B., DeCarlo, P. F., et al. (2011). Importance of secondary sources in the atmospheric budgets of formic and acetic acids. *Atmospheric Chemistry and Physics*, *11*(5), 1989–2013. https://doi.org/10.5194/acp-11-1989-2011

Peng, Q., Palm, B. B., Fredrickson, C. D., Lee, B. H., Hall, S. R., Ullmann, K., et al. (2021). Observations and modeling of NO_x photochemistry and fate in fresh wildfire plumes. *ACS Earth and Space Chemistry*, *5*(10), 2652–2667. https://doi.org/10.1021/acsearthspacechem.1c00086

Penner, J. E., Dickinson, R. E., & Neill, C. A. (1992). Effects of aerosol from biomass burning on the global radiation budget. *Science*, *256*(5062), 1432–1434. https://doi.org/10.1126/science.256.5062.1432

Petters, M. D., Carrico, C. M., Kreidenweis, S. M., Prenni, A. J., DeMott, P. J., Collett, J. L., Jr., & Moosmüller, H. (2009). Cloud condensation nucleation activity of biomass burning aerosol. *Journal of Geophysical Research*, *114*(D22), D22205. https://doi.org/10.1029/2009JD012353

Petters, M. D., Parsons, M. T., Prenni, A. J., DeMott, P. J., Kreidenweis, S. M., Carrico, C. M., et al. (2009b). Ice nuclei emissions from biomass burning. *Journal of Geophysical Research*, *114*(D7), D07209. https://doi.org/10.1029/2008JD011532

Petzold, A., Gysel, M., Vancassel, X., Hitzenberger, R., Puxbaum, H., Vrochticky, S., et al. (2005). On the effects of organic matter and sulphur-containing compounds on the CCN activation of combustion particles. *Atmospheric Chemistry and Physics*, *5*(12), 3187–3203. https://doi.org/10.5194/acp-5-3187-2005

Pósfai, M., Simonics, R., Li, J., Hobbs, P. V., & Buseck, P. R. (2003). Individual aerosol particles from biomass burning in southern Africa: 1. Compositions and size distributions of carbonaceous particles. *Journal of Geophysical Research*, *108*(D13), JD002291. https://doi.org/10.1029/2002JD002291

Pratt, K. A., Heymsfield, A. J., Twohy, C. H., Murphy, S. M., DeMott, P. J., Hudson, J. G., et al. (2010). In situ chemical characterization of aged biomass-burning aerosols impacting cold wave clouds. *Journal of the Atmospheric Sciences*, *67*(8), 2451–2468. https://doi.org/10.1175/2010JAS3330.1

Pratt, K. A., Murphy, S. M., Subramanian, R., DeMott, P. J., Kok, G. L., Campos, T., et al. (2011). Flight-based chemical characterization of biomass burning aerosols within two prescribed burn smoke plumes. *Atmospheric Chemistry and Physics*, *11*(24), 12549–12565. https://doi.org/10.5194/acp-11-12549-2011

Rattigan, O. V., Civerolo, K. L., Felton, H. D., Schwab, J. J., & Demerjian, K. L. (2016). Long term trends in New York: $PM_{2.5}$ mass and particle components. *Aerosol and Air Quality Research*, *16*(5), 1191–1205. https://doi.org/10.4209/aaqr.2015.05.0319

Reid, J. S., Koppmann, R., Eck, T. F., & Eleuterio, D. P. (2005). A review of biomass burning emissions part II: Intensive physical properties of biomass burning particles. *Atmospheric Chemistry and Physics*, *5*(3), 799–825. https://doi.org/10.5194/acp-5-799-2005

Roberts, G., Mauger, G., Hadley, O., & Ramanathan, V. (2006). North American and Asian aerosols over the eastern Pacific Ocean and their role in regulating cloud condensation nuclei. *Journal of Geophysical Research*, *111*(D13), D13205. https://doi.org/10.1029/2005JD006661

Rogers, H. M., Ditto, J. C., & Gentner, D. R. (2020). Evidence for impacts on surface-level air quality in the northeastern US from long-distance transport of smoke from North American fires during the Long Island Sound Tropospheric Ozone Study (LISTOS) 2018. *Atmospheric Chemistry and Physics*, *20*(2), 671–682. https://doi.org/10.5194/acp-20-671-2020

Rolph, G., Stein, A., & Stunder, B. (2017). Real-time environmental applications and display system: READY. *Environmental Modelling & Software*, *95*, 210–228. https://doi.org/10.1016/j.envsoft.2017.06.025

Rolph, G. D., Draxler, R. R., Stein, A. F., Taylor, A., Ruminski, M. G., Kondragunta, S., et al. (2009). Description and verification of the NOAA smoke forecasting system: The 2007 fire season. *Weather and Forecasting*, *24*(2), 361–378. https://doi.org/10.1175/2008WAF2222165.1

Sang, X. F., Gensch, I., Kammer, B., Khan, A., Kleist, E., Laumer, W., et al. (2016). Chemical stability of levoglucosan: An isotopic perspective. *Geophysical Research Letters*, *43*(10), 5419–5424. https://doi.org/10.1002/2016GL069179

Schroeder, W., Ruminski, M., Csiszar, I., Giglio, L., Prins, E., Schmidt, C., & Morisette, J. (2008). Validation analyses of an operational fire monitoring product: The Hazard Mapping System. *International Journal of Remote Sensing*, *29*(20), 6059–6066. https://doi.org/10.1080/01431160802235845

Schurman, M. I., Boris, A., Desyaterik, Y., & Collett, J. L. (2018). Aqueous secondary organic aerosol formation in ambient cloud water photo-oxidations. *Aerosol and Air Quality Research*, *18*(1), 15–25. https://doi.org/10.4209/aaqr.2017.01.0029

Schwab, J. J., Wolfe, D., Casson, P., Brandt, R., Demerjian, K. L., Husain, L., et al. (2016). Atmospheric science Research at Whiteface Mountain, NY: Site description and history. *Aerosol and Air Quality Research*, *16*(3), 827–840. https://doi.org/10.4209/aaqr.2015.05.0343

Seinfeld, J. H., & Pandis, S. N. (2016). *Atmospheric chemistry and physics: From air pollution to climate change* (3rd ed.), John Wiley & Sons, Inc.

Selimovic, V., Yokelson, R. J., McMeeking, G. R., & Coefield, S. (2020). Aerosol mass and optical properties, smoke influence on O_3, and high NO_3 production rates in a western U.S. City impacted by wildfires. *Journal of Geophysical Research: Atmospheres*, *125*(16), e2020JD032791. https://doi.org/10.1029/2020JD032791

Silva, P. J., Liu, D.-Y., Noble, C. A., & Prather, K. A. (1999). Size and chemical characterization of individual particles resulting from biomass burning of local southern California species. *Environmental Science & Technology*, *33*(18), 3068–3076. https://doi.org/10.1021/es980544p

Simoneit, B. R. T., Schauer, J. J., Nolte, C. G., Oros, D. R., Elias, V. O., Fraser, M. P., et al. (1999). Levoglucosan, a tracer for cellulose in biomass burning and atmospheric particles. *Atmospheric Environment*, *33*(2), 173–182. https://doi.org/10.1016/s1352-2310(98)00145-9

Sorooshian, A., Crosbie, E., Maudlin, L. C., Youn, J.-S., Wang, Z., Shingler, T., et al. (2015). Surface and airborne measurements of organosulfur and methanesulfonate over the western United States and coastal areas. *Journal of Geophysical Research: Atmospheres*, *120*(16), 8535–8548. https://doi.org/10.1002/2015JD023822

Sorooshian, A., Wang, Z., Coggon, M. M., Jonsson, H. H., & Ervens, B. (2013). Observations of sharp oxalate reductions in stratocumulus clouds at variable altitudes: Organic acid and metal measurements during the 2011 E-PEACE campaign. *Environmental Science & Technology*, *47*(14), 7747–7756. https://doi.org/10.1021/es4012383

Spracklen, D. V., Carslaw, K. S., Pöschl, U., Rap, A., & Forster, P. M. (2011). Global cloud condensation nuclei influenced by carbonaceous combustion aerosol. *Atmospheric Chemistry and Physics*, *11*(17), 9067–9087. https://doi.org/10.5194/acp-11-9067-2011

Srinivas, B., & Sarin, M. M. (2013). Light absorbing organic aerosols (brown carbon) over the tropical Indian Ocean: Impact of biomass burning emissions. *Environmental Research Letters*, *8*(4), 044042. https://doi.org/10.1088/1748-9326/8/4/044042

Stahl, C., Crosbie, E., Bañaga, P. A., Betito, G., Braun, R. A., Cainglet, Z. M., et al. (2021). Total organic carbon and the contribution from speciated organics in cloud water: Airborne data analysis from the CAMP2Ex field campaign. *Atmospheric Chemistry and Physics*, *21*(18), 14109–14129. https://doi.org/10.5194/acp-21-14109-2021

Stein, A. F., Draxler, R. R., Rolph, G. D., Stunder, B. J. B., Cohen, M. D., & Ngan, F. (2015). NOAA's HYSPLIT atmospheric transport and dispersion modeling system. *Bulletin of the American Meteorological Society*, *96*(12), 2059–2077. https://doi.org/10.1175/BAMS-D-14-00110.1

Straub, D. J., Hutchings, J. W., & Herckes, P. (2012). Measurements of fog composition at a rural site. *Atmospheric Environment*, *47*, 195–205. https://doi.org/10.1016/j.atmosenv.2011.11.014

Sullivan, A. P., Frank, N., Kenski, D. M., & Collett, J. L., Jr. (2011). Application of high-performance anion-exchange chromatography–pulsed amperometric detection for measuring carbohydrates in routine daily filter samples collected by a national network: 2. Examination of sugar alcohols/polyols, sugars, and anhydrosugars in the upper midwest. *Journal of Geophysical Research*, *116*(D8), D08303. https://doi.org/10.1029/2010JD014169

Sullivan, A. P., Frank, N., Onstad, G., Simpson, C. D., & Collett, J. L., Jr. (2011). Application of high-performance anion-exchange chromatography–pulsed amperometric detection for measuring carbohydrates in routine daily filter samples collected by a national network: 1. Determination of the impact of biomass burning in the upper midwest. *Journal of Geophysical Research*, *116*(D8), D08302. https://doi.org/10.1029/2010JD014166

Sullivan, A. P., Guo, H., Schroder, J. C., Campuzano-Jost, P., Jimenez, J. L., Campos, T., et al. (2019). Biomass burning markers and residential burning in the WINTER aircraft campaign. *Journal of Geophysical Research: Atmospheres*, *124*(3), 1846–1861. https://doi.org/10.1029/2017JD028153

Sullivan, A. P., May, A. A., Lee, T., McMeeking, G. R., Kreidenweis, S. M., Akagi, S. K., et al. (2014). Airborne characterization of smoke marker ratios from prescribed burning. *Atmospheric Chemistry and Physics*, *14*(19), 10535–10545. https://doi.org/10.5194/acp-14-10535-2014

Sun, W., Fu, Y., Zhang, G., Yang, Y., Jiang, F., Lian, X., et al. (2021). Measurement report: Molecular characteristics of cloud water in southern China and insights into aqueous-phase processes from Fourier transform ion cyclotron resonance mass spectrometry. *Atmospheric Chemistry and Physics*, *21*(22), 16631–16644. https://doi.org/10.5194/acp-21-16631-2021

Thepnuan, D., Chantara, S., Lee, C.-T., Lin, N.-H., & Tsai, Y. I. (2019). Molecular markers for biomass burning associated with the characterization of $PM_{2.5}$ and component sources during dry season haze episodes in Upper South East Asia. *Science of The Total Environment*, *658*, 708–722. https://doi.org/10.1016/j.scitotenv.2018.12.201

Tomaz, S., Cui, T., Chen, Y., Sexton, K. G., Roberts, J. M., Warneke, C., et al. (2018). Photochemical cloud processing of primary wildfire emissions as a potential source of secondary organic aerosol. *Environmental Science & Technology*, *52*(19), 11027–11037. https://doi.org/10.1021/acs.est.8b03293

Twohy, C. H., Toohey, D. W., Levin, E. J. T., DeMott, P. J., Rainwater, B., Garofalo, L. A., et al. (2021). Biomass burning smoke and its influence on clouds over the Western U. S. *Geophysical Research Letters*, *48*(15), e2021GL094224. https://doi.org/10.1029/2021GL094224

Tymstra, C., Stocks, B. J., Cai, X., & Flannigan, M. D. (2020). Wildfire management in Canada: Review, challenges and opportunities. *Progress in Disaster Science*, *5*, 100045. https://doi.org/10.1016/j.pdisas.2019.100045

Urban, R. C., Alves, C. A., Allen, A. G., Cardoso, A. A., Queiroz, M. E. C., & Campos, M. L. A. M. (2014). Sugar markers in aerosol particles from an agro-industrial region in Brazil. *Atmospheric Environment*, *90*, 106–112. https://doi.org/10.1016/j.atmosenv.2014.03.034

Urbanski, S. P. (2013). Combustion efficiency and emission factors for wildfire-season fires in mixed conifer forests of the northern Rocky Mountains, US. *Atmospheric Chemistry and Physics*, *13*(14), 7241–7262. https://doi.org/10.5194/acp-13-7241-2013

Vakkari, V., Kerminen, V.-M., Beukes, J. P., Tiitta, P., van Zyl, P. G., Josipovic, M., et al. (2014). Rapid changes in biomass burning aerosols by atmospheric oxidation. *Geophysical Research Letters*, *41*(7), 2644–2651. https://doi.org/10.1002/2014GL059396

Westerling, A. L. (2016). Increasing western US forest wildfire activity: Sensitivity to changes in the timing of spring. *Philosophical Transactions of the Royal Society B: Biological Sciences*, *371*(1696), 20150178. https://doi.org/10.1098/rstb.2015.0178

Wonaschuetz, A., Sorooshian, A., Ervens, B., Chuang, P. Y., Feingold, G., Murphy, S. M., et al. (2012). Aerosol and gas re-distribution by shallow cumulus clouds: An investigation using airborne measurements. *Journal of Geophysical Research*, *117*(17). https://doi.org/10.1029/2012JD018089

Wu, Y., Arapi, A., Huang, J., Gross, B., & Moshary, F. (2018). Intra-continental wildfire smoke transport and impact on local air quality observed by ground-based and satellite remote sensing in New York City. *Atmospheric Environment*, *187*, 266–281. https://doi.org/10.1016/j.atmosenv.2018.06.006

Xie, Y., Lin, M., & Horowitz, L. W. (2020). Summer $PM_{2.5}$ pollution extremes caused by wildfires over the Western United States during 2017–2018. *Geophysical Research Letters*, *47*(16), e2020GL089429. https://doi.org/10.1029/2020GL089429

Yang, C., Zhang, C., Luo, X., Liu, X., Cao, F., & Zhang, Y.-l. (2020). Isomerization and degradation of levoglucosan via the Photo-Fenton process: Insights from aqueous-phase experiments and atmospheric particulate matter. *Environmental Science & Technology*, *54*(19), 11789–11797. https://doi.org/10.1021/acs.est.0c02499

Yu, S. (2000). Role of organic acids (formic, acetic, pyruvic and oxalic) in the formation of cloud condensation nuclei (CCN): A review. *Atmospheric Research*, *53*(4), 185–217. https://doi.org/10.1016/s0169-8095(00)00037-5

Yuan, H., Wang, Y., & Zhuang, G. (2004). MSA in Beijing aerosol. *Chinese Science Bulletin*, *49*(10), 1020–1025. https://doi.org/10.1007/BF03184031

Zauscher, M. D., Wang, Y., Moore, M. J. K., Gaston, C. J., & Prather, K. A. (2013). Air quality impact and physicochemical aging of biomass burning aerosols during the 2007 San Diego wildfires. *Environmental Science & Technology*, *47*(14), 7633–7643. https://doi.org/10.1021/es4004137

Zhang, J., Lance, S., Brandt, R., Marto, J., Ninneman, M., & Schwab, J. (2019). Observed below-cloud and cloud interstitial submicron aerosol chemical and physical properties at whiteface mountain, New York, during August 2017. *ACS Earth and Space Chemistry*, *3*(8), 1438–1450. https://doi.org/10.1021/acsearthspacechem.9b00117

Zhang, X., Lin, Y.-H., Surratt, J. D., Zotter, P., Prévôt, A. S. H., & Weber, R. J. (2011). Light-absorbing soluble organic aerosol in Los Angeles and Atlanta: A contrast in secondary organic aerosol. *Geophysical Research Letters*, *38*(21), GL049385. https://doi.org/10.1029/2011GL049385

Zhao, R., Mungall, E. L., Lee, A. K. Y., Aljawhary, D., & Abbatt, J. P. D. (2014). Aqueous-phase photooxidation of levoglucosan—A mechanistic study using aerosol time-of-flight chemical ionization mass spectrometry (Aerosol ToF-CIMS). *Atmospheric Chemistry and Physics*, *14*(18), 9695–9706. https://doi.org/10.5194/acp-14-9695-2014

Zhou, S., Collier, S., Jaffe, D. A., Briggs, N. L., Hee, J., Sedlacek, A. J., Iii, et al. (2017). Regional influence of wildfires on aerosol chemistry in the western US and insights into atmospheric aging of biomass burning organic aerosol. *Atmospheric Chemistry and Physics*, *17*(3), 2477–2493. https://doi.org/10.5194/acp-17-2477-2017